

ACTA AERONAUTICA ET ASTRONAUTICA SINICA (SELECTED
ARTICLES)(U) FOREIGN TECHNOLOGY DIV WRIGHT-PATTERSON
AFB OH 17 JUN 87 FTD-ID(RS)T-0134-87

NL

F/G 1/2

63

END
8-87
DTK



MICROCOPY RESOLUTION TEST CHART
NATIONAL BUREAU OF STANDARDS 1963-A

2

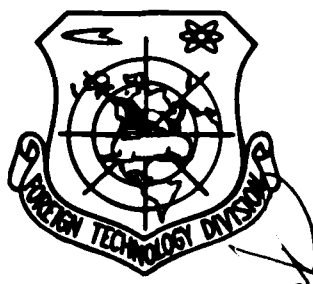
FTD-ID(RS)T-0134-87

DTIC FILE 1987

FOREIGN TECHNOLOGY DIVISION



ACTA AERONAUTICA ET ASTRONAUTICA SINICA
(Selected Articles)



DTIC
ELECTE
JUL 15 1987
S D E

Approved for public release;
Distribution unlimited.

AD-A182 447

87 7 14 040

HUMAN TRANSLATION

FTD-ID(RS)T-0134-87

17 June 1987

MICROFICHE NR: FTD87C000424

ACTA AERONAUTICA ET ASTRONAUTICA SINICA (Selected Articles)

English pages: 69

Source: Hangkong Xuebao, Vol. 7, Nr. 4, August 1986,
pp. 325-353

Country of origin: China

Translated by: SCITRAN

F33657-84-D-0165

Requester: FTD/TQTA

Approved for public release; Distribution unlimited.

THIS TRANSLATION IS A RENDITION OF THE ORIGINAL FOREIGN TEXT WITHOUT ANY ANALYTICAL OR EDITORIAL COMMENT STATEMENTS OR THEORIES ADVOCATED OR IMPLIED ARE THOSE OF THE SOURCE AND DO NOT NECESSARILY REFLECT THE POSITION OR OPINION OF THE FOREIGN TECHNOLOGY DIVISION

PREPARED BY

TRANSLATION DIVISION
FOREIGN TECHNOLOGY DIVISION
WPAFB OHIO

TABLE OF CONTENTS

Graphics Disclaimer	11
A Study of the Rotor Wake in Nap-Of-The-Earth, by He Chengjian and Gao Zheng	1
Study of the Separation Criterion for Steady 3-Dimensional Viscous Flows, by Lu Zhiyong, Deng Xueying, and Liu Mouji	17
Determination of Optimal Position of Actuators for Flexible Flight Vehicles, by Yuan Jianping and Chen Shilu	38
Numerical Simulation of a Flexible Aircraft Taking-Off and Landing on Uneven Runway, by Rui Yuting	53

Accession For		
NTIS	GRA&I	<input checked="" type="checkbox"/>
DTIC	TAB	<input type="checkbox"/>
Unannounced		<input type="checkbox"/>
Justification		
By		
Distribution/		
Availability Codes		
Avail and/or		
Dist	Special	
A-1		



GRAPHICS DISCLAIMER

All figures, graphics, tables, equations, etc. merged into this translation were extracted from the best quality copy available.

A STUDY OF THE ROTOR WAKE IN NAP-OF-THE-EARTH

325

He Chengjian and Gao Zheng

(Nanjing Aeronautical Institute)

SUMMARY This article does research into the primary aerodynamic problem with nap-of-the-earth flying-the ground vortex phenomenon. Through an analysis of rotor wake close to the ground, we have set up models, formulas, and methods for the calculation of its height off the ground, its longitudinal position, and its strength. Moreover, we have used these to calculate an induced speed distribution at the rotor disc. When we compared the results of calculations and experimental values, we arrived at relatively good agreement.

Table of Symbols

B	rotor tip loss coefficient
b_{eq}	equivalent rotor width at the rotor disc
R	rotor radius (m)
R_A	maximum vortex radius of ground vortex system (m)
Γ	rotor tip degree of vorticality
$(-)$	nondimensional coordinate parameters such as $\bar{h} = h/R$, $\bar{y} = y/QR$
C_T	rotor tensile coefficient
Γ_0	circulation distribution coefficient for ground vortex system
R_w	radius of the wake at a certain point on the ground (m)
S	comparative intercept area of rotor wake before and after collision with the ground
Ω	rotor angular velocity (1/s)

I. Introduction

We had done research early on concerning the ground effects of helicopter rotors. In the past, nap-of-the-earth flying for helicopters had been confined only to the short term phase of taking off and landing. Research on ground effects had been primarily concentrated on the aspects of rotor tensile strength and the power required.

In recent years, due to the requirement for the use of nap-of-the-earth flying by military helicopters in combat zones, there has been renewed interest in rotor ground effect problems in helicopter technology circles [1]. Continuous flight close to the earth at low speeds causes helicopters to be placed in a special aerodynamic environment and produces a series of new problems. Among these one finds involved, during periods of nap-of-the-earth flight, helicopter equilibrium, handling characteristics, flight capabilities, and interference from surrounding flow fields, as well as a number of other similar helicopter aerodynamic problems.

Rotor wake research is the foundation of the aerodynamics of helicopter nap-of-the-earth flight. It is only when one can set up a rotor wake model which is objective and realistic that it is then possible to realistically predict the aerodynamic characteristics of nap-of-the-earth flight.

In classical rotor ground effect theoretical research [2], the rotor wake is taken as fixed in order to describe the vortical system model. Making use of the projected image method to solve for the ground effect induction coefficient, it is possible to make reasonably good predictions of rotor capabilities in hover and during forward flight at relatively high speeds. However, application of this technique is limited in the low speed ranges encountered during nap-of-the-earth flight. The reason for this is that no account is taken of the relatively large wake deformation and surface vortical phenomena at such times. During the last few decades, people have achieved a very rich research understanding of the rotor aerodynamics of nap-of-the-earth flight. This is particularly true of the research

work done by the Boeing-Ford Helicopter Company (3) and Princeton University (4,5). This work makes a systematic discussion of ground vortical phenomena, and, from experimentation, presents their processes of occurrence, development, and disappearance. Princeton University also measured and recorded the rules governing changes in the locations of rotor flow fields and ground vortices during nap-of-the-earth flight. This is precious information for wake research. Reference [5] carried out theoretical research into rotor wakes, ground vortices, and mutual interference with the ground surface. It achieved relatively good results. Their work delved deeply into research concerning rotor aerodynamics during nap-of-the-earth flight and laid a valuable foundation.

326

In order to be able to carry out predictions of the aerodynamic characteristics of rotors during nap-of-the-earth flight, it is necessary to solve a key problem which is the calculation of the position and strength of ground vortices. The research which previous people have done has still not provided a method which is practically feasible and theoretically complete. This article presents a method for calculating the strength and position of ground vortices and rotor wakes as well as induced velocities. Because of this method, the calculated results and the experimentally measured data from Princeton University (5) mutually agree.

II. Surface Vortices

In recent decades, research from outside China has pointed out the phenomenon of ground vortices which appears particularly in nap-of-the-earth-flight. Experimentation [4] discovered that, from the appearance to the disappearance of ground vortices, the corresponding rate of rotor advance lay in a very narrow range from $\mu = 0.02$ to 0.05. At this time, the induced velocity distribution at the rotor blade disc changes abruptly (Fig. 1). It creates a deformation in the rotor aerodynamic characteristics. Its pitching moment follows changes in μ as shown in Fig. 2.

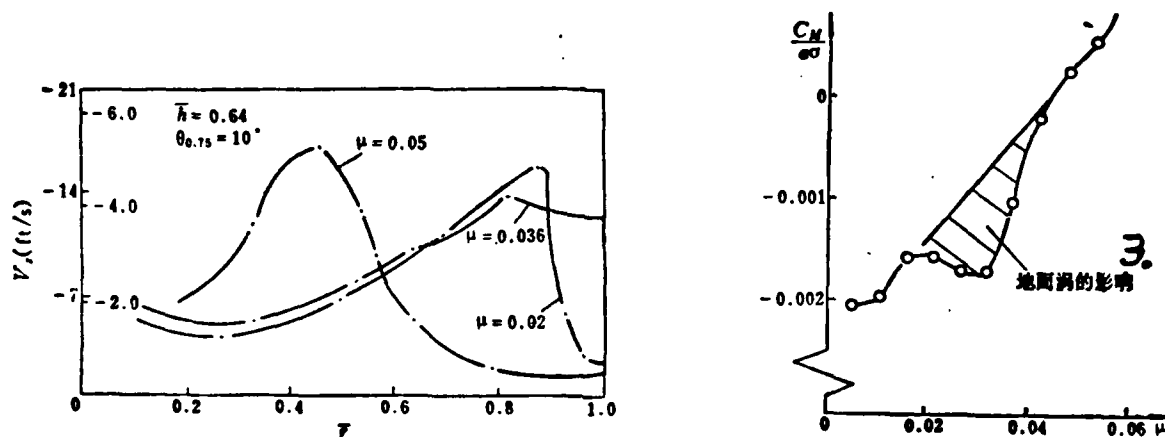


Fig. 1 The Relationship Between the Axial Component of the Rotor Disc Induced Velocity V_z and Its Corresponding Radial Position $r = r/R$ [5]

Fig. 2 Curve Describing Changes in the Pitching Moment In Terms of the Rate of Advance μ [7] (• Rate of Slope of the Lift Curve, σ Degree of Rotor Reality) 3. Influence of the Ground Vortex

The ground vortices are an accumulation, in the vicinity of the ground surface, of the rotor wake vortex (principally the rotor tip vortex) under the triple mutual influences of downward rotor wash flow, the oncoming flow encountering the flight and the ground surface. The rotor wake, due to the blocking effect of the ground surface, reduces speed and finally turns in the direction of the flow. It is dispersed along the ground surface in all directions. If the speed of forward flight is very low, the forward section of the rotor

wake flow still has a relatively large horizontal forward velocity along the ground. Because of the continuity of the flow movement, the wake flow disperses and reduces speed. At a certain point in the forward area, it mates with the corresponding wind. The supported wake vortices, then, accumulate at this spot forming the ground vortex. This vortex has an obvious effect on the surrounding flow fields and the aerodynamic characteristics of rotors.

1. Ground Vortex Vertical Position **G.**

Since ground vortices are the result of the mutual effects of the three factors of rotor wake flow, oncoming flight flows and the ground surface, the position of ground vortices can be solved on the basis of the principle of the superposition of movements.

After rotor wake flow collides with the ground, it assumes the forward wake flow movement of the wake vortex and reverses direction in terms of the oncoming flight flow. The horizontal velocity of gas flow close to the ground is taken from the superposition of the two. At the point where their flow speeds are the same (their combined speed is zero), the wake flow turns over and upward forming the ground vortex. The vertical position of this vortex can be solved for using the classical vortex system.

If we take the rotor coordinate system as our reference system (Fig. 3), the vertical speed of the surface flow is

$$V_s = V + v_{w_s} \quad (1)$$

In this equation, V is speed of flight. v_{w_s} is the rotor wake vortex and its horizontal induced velocity as projected on the vertical plane of symmetry rising from the ground surface. On the basis of classical rotor vortex flow theory [6] and projection methods, one has

$$v_{\theta} = -\frac{R}{2\pi} \int_0^{2\pi} \frac{d\Gamma}{dl} \left[\frac{\cos\theta(R\cos\chi - h)}{R_p(R_p + B_p)} - \frac{\cos\theta\cos\chi}{R_p + B_p} \right] d\theta \quad (2)$$

In this equation $\frac{d\Gamma}{dl}$ is the amount of circulation for a unit length along the direction of the center line of the vortex

$$\begin{aligned} R_p &= \sqrt{R^2 + G_s^2 + h^2 + 2RG_s\cos\theta} \\ B_p &= (G_s + R\cos\theta)\sin\chi - h\cos\chi \\ R_{p1} &= \sqrt{R^2 + (G_s + h\tg\chi)^2 + 2R(G_s + h\tg\chi)\cos\theta} \\ B_{p1} &= (G_s + R\cos\theta + h\tg\chi)\sin\chi \end{aligned}$$

At the place where the ground vortex is formed one should have $V_s = 0$, that is,

$$V = -v_{\theta} \quad (3)$$

This equation determines the vertical position G_{s0} of the ground vortex. At this point, it is necessary to point out that the wakes in the various equations above must be used with correction values for the angle of incline χ of the vortical core.

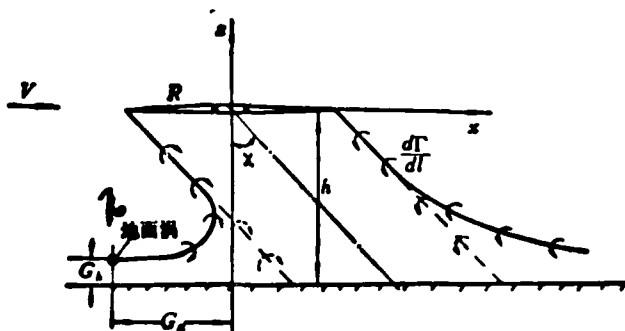


Fig. 3 Rotor Coordinate System 1. Ground Vortex

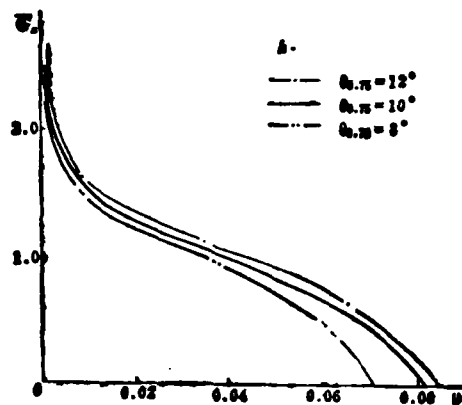


Fig. 4 Curve Expressing Changes in the Vertical Position G_v of the Ground Vortex as a Function of μ ($\theta_{0.75}$ is the Overall Distance)

32

G_v is an important parameter describing ground vortices. Fig. 4 presents changes in G_v as a function of the rate of forward rotor movement. In all situations, G_v is always a monotonic reduction function of μ . The diagrams show the effect of the overall distance $\theta_{0.75}$ on the position of the ground vortex. The larger the overall distance is, the greater are the momentum and the kinetic energy of the downward wash. The ground vortex then appears in a place even farther to the front of the rotor.

Although, when we solved for the vertical position G_v of the ground vortex, we did not consider the influence of the ground vortex itself, it is true, however, that classical vortical systems already calculate in that portion of the near ground wake which goes to form the ground vortex. Because of this, we get a certain compensating factor. From a comparison of the calculated values presented in Fig. 5 and experimentally measured values, we can see that the degree of agreement between the two is quite satisfactory.

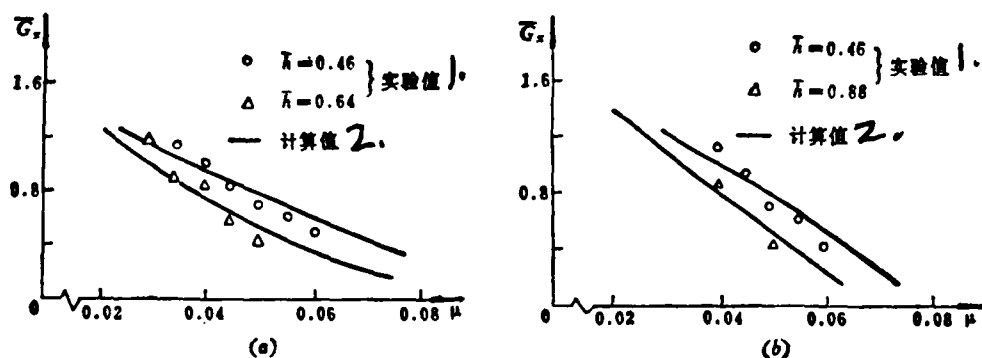


Fig. 5 A Comparison Between Values Calculated for G_x on the Basis of the Methods of This Article and Experimental Values 1. Experimental Values 2. Calculated Values

(a) $\theta_{0.75} = 10^\circ$, (b) $\theta_{0.75} = 12^\circ$.

2. The Height Off the Ground G_h of Ground Vortices

According to what we see in Fig. 6, the rotor wake flow flows down at an angle toward the ground at velocity V_1 . In order to simplify this, let us assume that, after the wake flow contacts the ground, it divides into two longitudinal flow movements along the ground. The thickness of the forward branch is G_h . The thickness of the rearward branch is h_{h_2} . When we pay attention to applying the principles of momentum and continuity equations, we make a three dimensional correction to the wake flow. If we do not figure in the ground friction force, it is possible to write an x -direction momentum equation for the control body shown in the diagram.

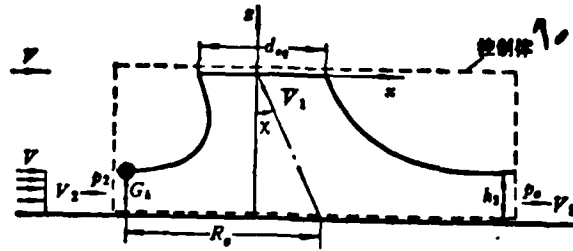


Fig. 6 Derivation of Momentum Equation for Control Body 1. Control Body

$$\frac{p_1 - p_2}{\rho Q^2 R^2} \bar{G}_1 = (\bar{h}_2 \bar{V}_2^2 - \bar{G}_2 \bar{V}_2^2) - \frac{\bar{d}_{cg}}{R_0} \bar{V}_1^2 \sin \alpha \quad (4)$$

The continuity equation is

$$\bar{G}_1 \bar{V} + \bar{h}_2 \bar{V}_2 = \frac{\bar{d}_{cg}}{R_0} \bar{V}_1 \quad (5)$$

If we make equations (4) and (5) simultaneous, and, we take into consideration the energy losses which occur when the rotor wake collides with the ground surface, we can go through mathematical operations and obtain

329

$$\bar{G}_s = \frac{\bar{d}_{s0}(K_s - \sin\chi)}{\bar{R}_s \left[\frac{1}{2}(K_s^2 + \sin^2\chi) + K_s \sin\chi \right]} \quad (6)$$

In this

$$\begin{aligned} d_{s0} &= \frac{\pi}{2} B^2 \\ K_s &= \left\{ S_s^2 + S_s \left[\frac{2C_T \sin^2\chi}{\mu} - \cos^2\chi - 2\cos\chi(S_s - 1) \right] \right\}^{1/2} \\ S_s &= (B/\bar{R}_s)^2, \quad \bar{R}_s = \bar{G}_s + h \tan\chi \end{aligned}$$

We should pay attention to the fact that the rotor blade tip vortex is only distributed on the wake flow surface. Because of this, the thickness of the branch flow in the forward direction after the wake flow contacts the ground here is then the height of the ground vortex which we solve for. Fig. 7 shows a comparison of calculated values and experimental values. The two agree.

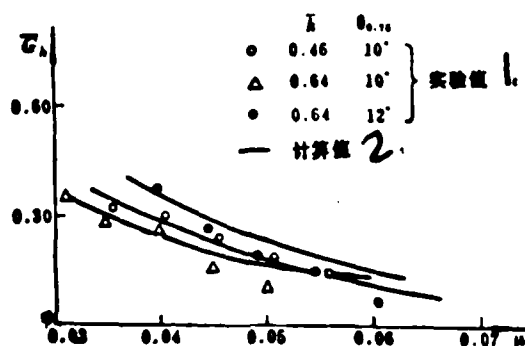


Fig. 7 A Comparison of Experimental Values and Values for h as Calculated According to the Method of This Article 1. Experimental Values 2. Calculated Values

3. Ground Vortex Strength Γ_0

Let us assume that the wake vortex which avoids the rotor blade tip takes the form of a vortical ring and moves downward following the wake flow. At a place a certain distance above the ground, it changes and is only dispersed in a horizontal plane. The forward section of the rotor tip vortical ring moves slowly due to its windward position. The rear section moves at high speed because it is moving with the wind. In order to simplify calculations, take the wake which is shown close to the ground by the planar ring-shaped vortex of the continuity distribution for the amount of circulation (Fig. 8) and assume that its circulation distribution is

$$\frac{d\Gamma}{d\rho} = \begin{cases} 0 & (\rho < R) \\ \frac{d\Gamma}{dl} \left[1 + \frac{1-f_r}{R_*} \rho \cos\theta_* \right] & (R \leq \rho < R_*) \end{cases} \quad (7)$$

In this $f_r = V_i/V_*$.

This type of distribution reflects the principle of longitudinal distribution of the amount of circulation in close wakes which says that the front is large and the rear is small.

In Fig. 8, this type of planar vortex system, due to the mutual effects of vortex rings, has edges which are unstable, and will roll up. The forward peak of this vortex system is at the place where the oncoming flow of flight and the rotor wake come together. Under limits imposed by the ground boundary, the wake flow accumulates at this point, turns upward and rolls to form a ground vortex.

The ground vortex, on the one hand, receives a continuous replenishment from the rotor tip vortex in the rotor down flow. On the other hand, it dissipates its amount of vorticality to the surroundings due to gas flow viscosity. When the processes of vortex building and dissipation reach a dynamic equilibrium, then, the surface vortex is set up and maintained at a certain strength. Because of this,

$$\Gamma_s = f_s \int_R \frac{d\Gamma}{d\rho} d\rho$$

(5)

The parameter f_s is called the surface vortex strength parameter. It expresses quantitatively the degree of vortical confluence in the wake. The bigger f_s is the greater is the rotor wake vortex amalgamation forming a concentrated vortex. $f_s = 0$ is the critical value. One can see that, at this point, it is not possible for wake vortices to unite to form ground vortexes.

330

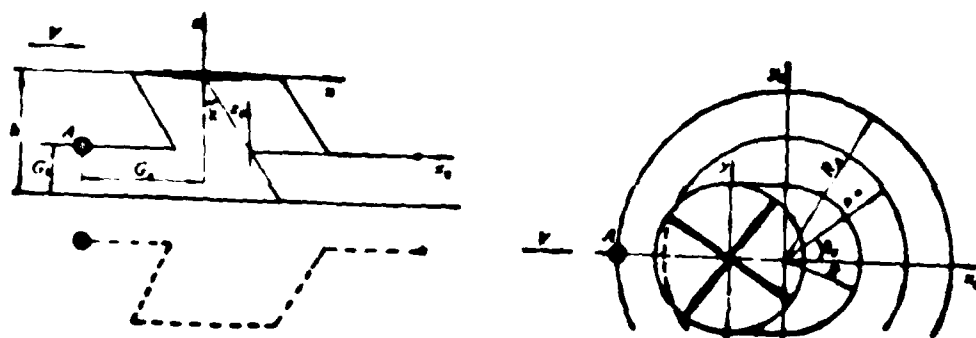


Fig. 8 The geometrical relationships of rotor wakes close to the ground

On the basis of the condition that ground vortexes are stationary in reference to the rotors concerned, it is possible to solve for f_s . According to the principle of superposition, the horizontal velocity at the position of the ground vortex should be

$$V_s = V + v_{w1} + v_{w2} + v_{w3}$$

(6)

In this v_{Ax}, v_{Ax1}, v_{Ax2} are respectively the components of induced velocity along the x axis caused at that point in the rotor wake in response to changes in the vortical system and its projection, the planar vortical system projection, and the ground vortex projection. Since the ground vortex and the rotor are stationary relative to each other, then, $V_{Ax} = 0$. From this, it is possible to obtain the strength coefficient for the ground vortex, which is,

$$I_s = -\frac{2\pi(V + v_{Ax} + v_{Ax1})}{G_s \int_0^{\pi} \frac{d\Gamma}{dl} I_{s1} d\theta_s} \quad (10)$$

In this

$$I_{s1} = \frac{1}{2}(R_s - R)\cos\theta_s[(1 - f_r)(R_s + R)\cos\theta_s + 2R_s]/T_s$$

$$T_s = \sqrt{R_s^2 - 2R_s W_s + P_s}$$

$$W_s = -R_s \cos\theta_s$$

$$P_s = R_s^2 + 4G_s^2$$

$$R_s = G_s + (h - G_s)\tan\chi$$

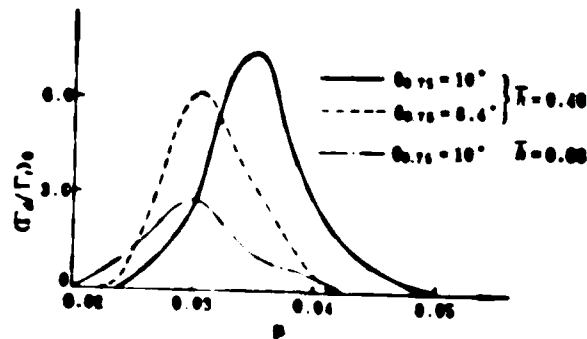


Fig. 4 The Curve for $\sigma_d(G_s)$ in Terms of Changes in G_s

Fig. 9 presents the principles governing the average values of the ratio between surface vortex strength and blade tip vortex strength in response to changes in μ . It also presents the influences of the height of the rotor off the ground and its overall distance. One can see that ground vortices exist only in a very narrow range of values of μ . Moreover, when μ has a certain value, there is a maximum value. The greater \bar{h} is or the smaller $\theta_{0.7}$ is, the smaller is the peak value for $(\Gamma_s/\Gamma_t)_0$. Moreover, values of μ which correspond to these peak values are also small. These principles of change and the patterns of experimental observations agree with each other. It would be reasonable to make an analysis of this. Unfortunately, there are still no data from experimental measurements with which to make comparisons.

According to the position and strength of ground vortices as presented in this article, the results from an application of free vortical system methods to calculate rotor wake and the induced velocities caused by it in nap-of-the-earth flight demonstrate that the methods in this article for calculating the strength and position of ground vortices can be applied to an analysis of the aerodynamic characteristics of rotors.

At many places in this article, we have quoted the experimentally measured data from reference [5] in order to confirm the calculation results in this article. Because of this, we wish to give our special thanks to Professor H.C. Curtiss, Jr. and Dr. Sun Mao.

REFERENCES

- (1) 高正, 直升机的贴地飞行, NHJB-1057, 南京航空学院, (1984).
- (2) Hayson, H H, Theoretical Study of the Effect of Ground Proximity on the Induced Efficiency of Helicopter Rotors NASA TM X-71061, May (1977).
- (3) Sheridan, P F and Wiesner, W, Aerodynamics of Helicopter Flight near the Ground Paper No 77-33-04, Presented at the 33rd Annual National Forum of the American Helicopter Society, Washington, D C, May (1977).
- (4) Curtiss, H C Jr, Sun M, Putman, W F and Harker, E J Jr, Rotor Aerodynamics in Ground Effect at Low Advance Ratios Presented at the 37th Annual Forum of the A H S, New Orleans, Louisiana, May (1981).
- (5) Sun Mao, A Study of Helicopter Rotor Aerodynamics in Ground Effect at Low Speed Ph D. Thesis, Dept of Mechanical and Aerospace Engineering, Princeton University, May (1983).
- (6) 王德寿, 升力矩的广义相似理论, 西北工业大学, (1962).
- (7) Harker, E J Jr, Experimental Investigation of the Ground Vortex Phenomenon in Helicopter Flight near the Ground 1981 Midwest Regional Lichten Award Winning Paper (AHS), Jan (1981).

- [1] Gao Zheng; "Nap-Of-The-Earth-Flight in Helicopters," NHJB-1857, Nanjing Aeronautical Institute, (1984).
- [6] Wang Shicun; "Generalized Vortical Flow Theory for Lift Blades," Northwestern Industrial College, (1962)

A STUDY OF THE ROTOR WAKE IN NAP-OF-THE-EARTH

He Chengjan and Gao Zheng

(Nanjing Aeronautical Institute)

Abstract

In this paper an investigation of the ground vortex, the significant aerodynamic phenomenon in rotor aerodynamics on nap-of-the earth, is carried out. Based on the analysis of the rotor wake near the ground, a theoretical method, including the analytical model, the formulae and the computer program, has been established which can be used for calculation of the ground vortex—the longitudinal position, the height above the ground and its strength. By using a free wake model, with the ground vortex taken into account, the distribution of induced inflow at the rotor disc is also calculated. All computational results are compared with available experimental data and found in good agreement.

STUDY OF THE SEPARATION CRITERION FOR STEADY
3-DIMENSIONAL VISCOUS FLOWS

332

Lu Zhiyong, Deng Xueying, and Liu Mouji

(Beijing Institute of Aeronautics and Astronautics)

SUMMARY This article takes the topological principles of singularity point theory as a starting point and explains the existence of half saddle points on the cross section flow lines perpendicular to the lines of separation and the cross section of the object. It goes on to explain that the perception by such people as Lighthill that extreme limit flow lines must raise up before the separation flow lines is not reasonable. The reasonable way of explaining the phenomena should be that the extreme limit flow lines are always coincident with shear stress lines. It is only after entering points of singularity that extreme limit flow lines finally raise up and leave the surface of the object. Finally, this article demonstrates that the simpleminded application of two-dimensional separation criteria to three-dimensional separation situations is inadequate. Moreover, it presents formulae to express three-dimensional separation criteria.

Introduction

Following increases in the flight speed of aircraft missiles, in order to appropriately respond to the requirement to raise the lift-drag ratio for transonic and supersonic speeds, it is necessary to select for use thin aircraft wings having large back sweeps and small length to width ratios. The fuselage used is also relatively long and thin in order to facilitate the lowering of wave drag as well as trim drag. With thin wings and large angles of back sweep it is very easy to create three dimensional separation. Besides this, because of the fact that the capabilities of fighters and missiles have increased without ceasing, it is often necessary, with even larger windward angles, to carry out flight maneuvers, leading to strong three-dimensional separation flows appearing on the back wind surfaces of the aircraft. Because of this, research concerning three-dimensional separation has become a totally obligatory requirement.

Research into three-dimensional separation has only been done in the last twenty or thirty years. However, at its earliest, it can be traced back to 1948, when Sears, in an article on the "boundary layers of drift cylinders" presented the concept of what he called extreme limit flow lines. He recognized that adhering closely to the surface of objects there were flow lines existing which were like a very thin sleeve around the object. Beginning from the 1950's, corresponding to the development of aircraft missiles at that time, problems of three dimensional separation began to attract the serious attention of people. E.C. Maskell, on the basis of extensive experiments with oil flow, drew together the experimental results of other people at the time and presented a general definition of three dimensional separation (1). Such men as R. Legendre (1956) and M.J. Lighthill (1963), basing themselves on flow line equations and shear stress line equations, applied the qualitative theory of differential equations and presented the singularity point topologic method of analysis. On the basis of this point of view, the multivarious flow states on walls were determined by nothing more than a limited point of singularity from flow line equations or surface shear stress line equations and the equations mutually interconnecting them. These points of singularity all had clear physical significance. According to the rules of topology, two flow states which have different configurations, if they have the same number of types of points of singularity and connecting equations, are the same and the two flow states are topologically equivalent. Because of this, utilization of singularity point topological analysis makes it possible to interpret the significance of the appearance of points of singularity in flow configurations, to analyze flow configurations, and to predict possible new flow configurations [2].

Peake, Tobak (2), Dallman (1980) (4) and K.C. Wang, in recent years, have utilized the topological concept of points of singularity to analyze many types of flow configurations on aircraft, forming one important part of the contents of the qualitative research on three-dimensional separation. Due to the introduction of topological points of similarity, the flow configuration analysis based on experimental observations, which had been used in the past, developed in the direction of the utilization of mathematical tools. Even to the present day, the use of numerical value methods to solve for three-dimensional separation flows is still extremely difficult. Because of this, qualitative research is still a very important path to be pursued. Through it, it is possible to understand the structure of separation flows. It is also possible to make progress toward presenting a simplified mathematical model to serve in numerical value calculations. This article concentrates on the discussion of the form and criteria of three-dimensional separation. 333

I. Two Different Types of Models in Research on Three-Dimensional Separation

In order to understand the special points of three-dimensional separation, we will first reconsider for a moment the situation in two-dimensional steady state separation. Two-dimensional steady state separation is a type of singularity point separation. The point of separation is located at the intersection of flow lines, showing the formation of half saddle points (Fig. 1). The wall surface flow lines flow into the point of separation from two sides. After they flow together, the flow lines and the wall surfaces form an open wall surface with a certain included angle. According to the definition for points of singularity, and, given the condition that the normal velocity near separation points is not zero, it is possible to derive the separation criteria presented below [3,5].

$$\frac{\partial u}{\partial z} = 0, \quad \frac{\partial^2 u}{\partial x \partial z} < 0$$

(1)

In these, x runs along the surface of the object. z is a direction normal to the surface of the object. u is the velocity component in direction x (Fig. 1).

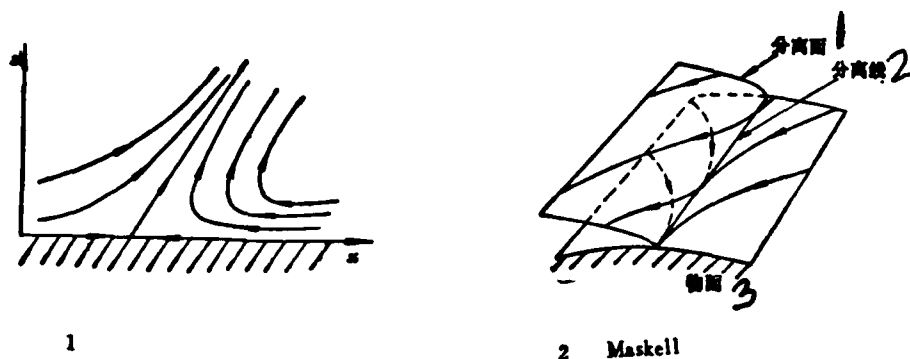


Fig. 1 A Diagram of Two-Dimensional Separation

Fig. 2 Maskell Three-Dimensional Separation Model 1. Separation Surface 2. Separation Lines 3. Object Surface

As far as three-dimensional separation is concerned, there are always two different points of view (models) in existence, that is,

1. The Maskell three-dimensional model [1]. In 1955, in his famous essay "Three-Dimensional Separation Flow," he first presented the idea that separation lines are an envelope of extreme limit flow lines (Fig. 2). The extreme limit flow lines flow toward the separation lines from the two sides of the separation lines. Moreover, the same separation flow line cuts itself. After this, it leaves the surface of the object and forms a three-dimensional separation flow surface (it is a one flow surface.) Separation

surfaces come in two forms, three-dimensional separation gas bubbles and free vortical surfaces (Fig. 3). The gas bubble-form separation line normally connects saddle point-form points of singularity. At points of singularity, $\frac{\partial u}{\partial z} = \frac{\partial v}{\partial z} = 0$. This is equivalent to the disappearance of shear stress, that is, $\tau_x = \tau_y = 0$. On separation lines, besides this type of independent point of singularity, they are all ordinary points. At the locations of ordinary points $\frac{\partial u}{\partial z}$ and $\frac{\partial v}{\partial z}$ cannot both be zero at the same time, that is, the shear stress cannot be zero. Therefore, at ordinary point locations, one has at least two extreme limit flow lines mutually intersecting to form a peak point. The separation lines are the tracks of this type of peak point.

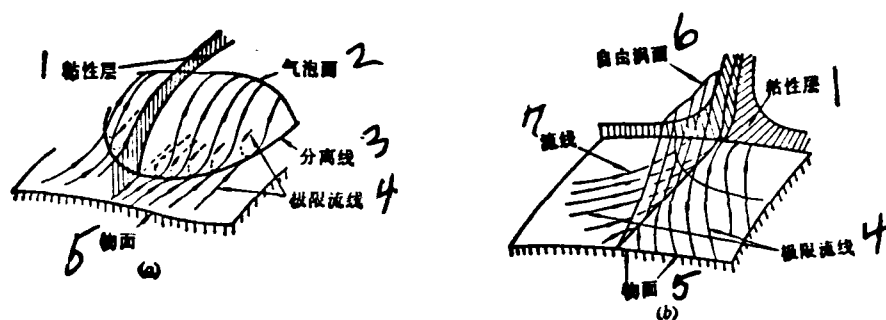


Fig. 3 Two Different Types of Separation Forms (a) Gas Bubble (b) Free Vortical Surface 1. Viscous Layer 2. Gas Bubble Surface 3. Separation Line 4. Extreme Limit Flow Lines 5. Surface of Object 6. Free Vortical Surface 7. Flow Lines

According to Maskell's definition of separation lines and separation surfaces, it is possible to derive the fact that the cross section flow lines on the cross section plane perpendicular to separation lines and the object surface intersect each other at points on the flow lines and cross sections to form semi-saddle points (Fig. 4). This is similar to the situation with two-dimensional separation.

The cross section of extreme limit flow lines with the plane xoz forms a point of singularity at point o . . When there is separation, it is necessary to have a normal velocity to leave the surface of the object. Because of this, equation (1) is satisfied at point o . . Flow lines on the separation surface cut across separation lines. They do not cut across the surface of the object. Because of this, the separation surface forms an angle of a certain size with the surface of the object.

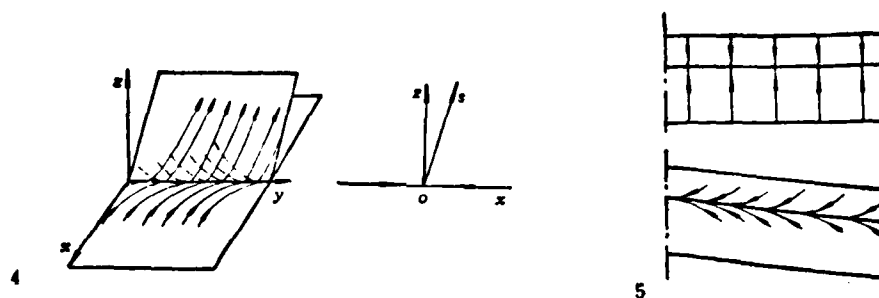


Fig. 4 Maskell Separation Model and Cross Section Flow Lines y - - Separation Line Direction, z - - Direction Normal to the Surface of the Object, x - - Positioned on the Surface of the Object Perpendicular to y .

Fig. 5 Separation Lines on Two-Dimensional Straight Aircraft Wings and Sweptback Wings

Obviously, Maskell's concept of three-dimensional separation can be drawn out as an extension of two-dimensional separation. If we assume a two-dimensional straight aircraft wing having on it a separation line parallel to the forward edge, when the forward edge of the wing is swept back, the two-dimensional separation line then becomes Maskell's three-dimensional separation line. It is equivalent to two-dimensional separation with the addition of a component for the direction of development (Fig. 5).

Maskell's separation model finds important application in research on three-dimensional separation. In recent decades it has been extensively quoted by people. In oil flow spectrum analysis, he presented methods for determining lines of separation on object surfaces as well as auxiliary lines. Moreover, he was able to connect the flow configurations for object surfaces to the flow configurations in the air.

2. The Lighthill and Peake-Tobak model. After the 1960's, people became more and more interested in the flow configurations for aircraft at large windward angles. At such times, leeward surfaces often show the appearance of very complicated separation flows, including vortical flow forms and point vortices. According to Maskell's model, there was no way to solve for these. Because of this, these types of point vortices were often seen as oil vortices and were considered to be phenomena produced by oil flows. Observations of air flow configurations demonstrate that point vortices on the surfaces of objects (also a type of separation structure point) are start points for simple root filament vortices, and are often the start points for the vortical cores of three-dimensional separation vortices (Fig. 6).

In the Maskell model, extreme limit flow lines form peak points at points of separation. At one point, there are, simultaneously, two upward flow lines crossing. Moreover, the lines of separation cut each other. Lighthill [2] demonstrated that, in the vicinity of lines of separation, it is not possible for extreme limit flow lines to mutually intersect separation lines—that they lift off the surface of objects in front of the lines of separation. Because of this, such people as Lighthill and Peake-Tobak did not use extreme limit flow lines to define and analyze the flow characteristics in the vicinity of three-dimensional separation lines. They made use of shear stress lines to make their definitions and analysis. They recognize that shear stress lines exist everywhere on the surface of objects and that shear stress fields on the surface of objects are continuous vector quantity fields. The extreme limit flow line equation is

$$\lim_{z \rightarrow 0} dy/dx = v/u \quad (2)$$

When $z \rightarrow 0$, from non-glide conditions on the surface of the object $v \rightarrow 0$, $u \rightarrow 0$ and L'Hopital's law

$$dy/dx = \left(\frac{\partial v}{\partial z} \right)_{z=0} / \left(\frac{\partial u}{\partial z} \right)_{z=0} \quad (3)$$

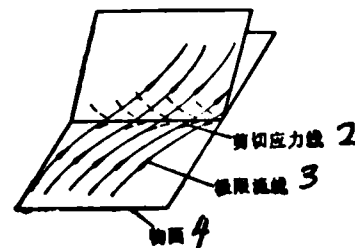
From half ton formulas $\tau_x = \mu \left(\frac{\partial u}{\partial z} \right)_{z=0}$, $\tau_y = \mu \left(\frac{\partial v}{\partial z} \right)_{z=0}$.
Therefore, equation (3) can be written as

$$dy/dx = \tau_y / \tau_x \quad (4)$$

The shear stress line equation (4) and the extreme flow line equation (3) correspond completely. In the vicinity of lines of separation, extreme limit flow line equations do not represent actual flow lines. They simply represent their projections (this point will be discussed later.) Because of this, Lighthill only uses equation (4) to discuss separation.



6



7 Lighthill

Fig. 6 Point Vortices on the Surface of Objects 1. Point Vortex

Fig. 7 Lighthill Separation Model 2. Shear Stress Line 3. Extreme Limit Flow Line 4. Object Surface

Starting from the point of view of a topological analysis of points of singularity, Lighthill and Peake-Tobak recognize that lines of separation are basically shear stress lines. The starting points for lines of separation are saddle points, and their end points are the end points of the separation. On the two sides of the separation line, the shear stress lines take the separation line as their asymptote leading to convergence. They finally flow together at the end point of the separation (Fig. 7).

3. The debate concerning the definition of separation lines. The debate over whether lines of separation are asymptotes or envelopes is still continuing up to the present. Because of the fact that, in such experiments as those involving oil flows, the resolution in the vicinity of the separation lines is limited, it cannot be determined whether they are asymptotic or they cross. Mathematically, it is at present not possible to directly solve the N-S equations involved in three-dimensional separation problems. Inside China, Zhang Hanxin-basing himself on a certain separation model-maintains that, as far as boundary layer equations are concerned, separation lines are an envelope, but, in terms of N-S equations, separation lines are asymptotes. Moreover, he recognizes that, on a cross section perpendicular to the separation lines, cross section flow lines, at points of intersection between separation lines and cross sections, should be saddle points. Therefore, he takes two-dimensional criteria concerning separation and uses them on three-dimensional separation flows [6].

II. A Discussion of Singularity Point Characteristics on Cross Sections Perpendicular to Three-Dimensional Separation Lines

The models of people like Lighthill and the Maskell model are different. They maintain that the extreme limit flow lines curl up

in the vicinity of separation lines and never intersect separation lines at any point. They do not even intersect each other. In the vicinity of the separation line projections, they follow the direction of the surface shear stress lines and finally flow together at the end point of the separation. If they are perpendicular to the separation lines and the plane of the surface of the object, then, the flow line orientation of that plane is not able to form half saddle points (Fig. 8). Because of this, in topological methods of analysis for separation points, it is necessary to carry out adjustments of the relationships of extreme limit flow lines and shear stress lines in the vicinity of separation lines in order to make them reasonable.



Fig. 8 In the Model of Such People as Lighthill, Cross Section Flow Lines Are Not Able to Form Half Saddle Points

Fig. 9 Delta Wing Cross Section Flow Line Flow Configurations Adjacent to Body

1. Points of singularity perpendicular to the plane of separation flow lines. Maskell is different from the topological analysis model of separation, and the two of them cannot be confused. In a topological analysis of points of singularity, one should make the points of separation on flow line cross sections points of singularity-half saddle points.

According to the theory for the topological analysis of points of singularity [3], when simply connected domain bodies are pinned to intercept each other, on these planes, the flow lines should satisfy the topological rule

$$\left(\Sigma_0 + \frac{1}{2} \Sigma_0'\right) - \left(\Sigma_1 + \frac{1}{2} \Sigma_1'\right) = -1$$

5

The subscripts N, N' stand for nodal points and semi-nodal points. The subscripts S, S' stand for saddle points and half saddle points. Σ represents the singularity point number.

Concerning the flow configuration close to the body (Fig. 4), cross section flow lines have only two half saddle points, satisfying equation (6).

As far as delta wings with front edge vortices are concerned (Fig. 10), the forward edge is the half saddle point for separation lines on the cross sections. In the interval between, on the cross section close to the lines, there are also half saddle points. Because of this equation (6) is satisfied.

From the examples given above, one can see that, in a topological analysis of points of singularity, intersection points between separation lines and cross sections are half saddle points. With this being the case, now one understands the structure of separation surfaces and the formation of half saddle points is a question worthy of discussion.

2. The formation of separation surfaces in topological analyses of points of singularity. In the Maskell model, separation planes are formed from extreme limit flow lines separating from the surface of objects. In the Lighthill model, separation surfaces are formed from the turning up of extreme limit flow lines. They should come from the origination point of upper flow points of singularity and separation lines.

Figure 10 shows a cone with a spiral on its base. To the right, a coordinate system with axes S and S' displays a spiral curve that winds around the S axis, with arrows indicating the direction of the spiral.

Fig. 10 Points of singularity in space - a saddle point - Node
Point - Saddle Point - Node - Node - Node - Node - Node - Node -
Node - Node

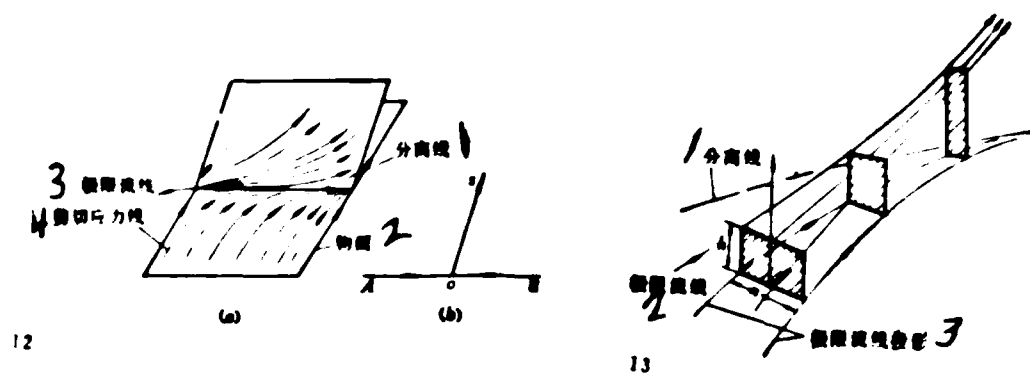


Fig. 12. Formation of separation surfaces and free surface in flow field: 1. Separation Line; 2. Free Surface; 3. Extreme Limit Flow Line; 4. Shear Stress Line.

Fig. 13. Separation Line Forward Flow Tube Characteristics: 1. Separation Line; 2. Extreme Limit Flow Line; 3. Extreme Limit Flow Line Projection.

3. A discussion of the characteristics of extreme limit flow lines in the vicinity of separation lines. The model of flow proposed by Lighthill recognizes that extreme limit flow lines, in the vicinity of separation lines, have projections which coincide with the shear stress lines for the same surface. They finally pass through the separation nodal point. However, the extreme limit flow lines themselves do not pass through the separation nodal point. This type of viewpoint should be corrected. Lighthill's demonstration concerning the upward turning of extreme limit flow lines in the vicinity of separation lines is as shown below.

As is shown in Fig. 13, on the surface of the object, we select an orthogonal curve-coordinate system. ξ and η are parallel to the surface of the object. ζ is normal to the surface of the object. On the surface of the object $\zeta = 0$. The extreme flow line equation or surface shear stress line equation is

$$h_1 d\xi/\tau_{\xi\xi} = h_2 d\eta/\tau_{\eta\eta} \quad (6)$$

In this h_1 and h_2 are Lamé coefficients.

$$\tau_{\xi\xi} = \mu (\partial u / \partial \xi)_{\zeta=0}, \quad \tau_{\eta\eta} = \mu (\partial v / \partial \eta)_{\zeta=0} \quad (7)$$

They are respectively parallel to the components of ξ , η . We assume that Δ is the distance between extreme limit flow lines. h is the height of the flow tube. The amount of mass flowing through the mass flow tube is

$$m = \rho h n u$$

In this, ρ is density, u is average velocity. Surface shear stress is

$$\tau_s = \mu \left(u / \frac{h}{2} \right)$$

The result is

$$h = \tau_s / 2\mu$$

Because of this

$$m = h^2 \pi \tau_w / 2 = \text{const}$$

$$h = C \left(\frac{v}{\pi \tau_w} \right)^{1/2}, \quad v = \mu / \rho \quad (10)$$

When approaching separation lines, $h \rightarrow \infty$. Because of this, in the vicinity of three-dimensional separation lines, the flow lines inside flow tubes must turn up. This includes extreme limit flow lines.

The proof described above explains that the raising of flow tubes in the vicinity of separation lines is correct. However, it recognizes that the separating of extreme limit flow lines from the surface of objects is not certain. If it follows the movement upward, then its lower surface must also have flow lines. This is contradictory to the definition of extreme limit flow lines. Because of this, extreme limit flow lines will not leave the surface of the object. It is only at the location of points of singularity that extreme limit flow lines flow together. After that, they separate from the surface of the object at a given angle. Fig. 14 presents the patterns for extreme limit flow line separation from the surface of objects in the Maskell, Lighthill models as well as for the model presented in this article.

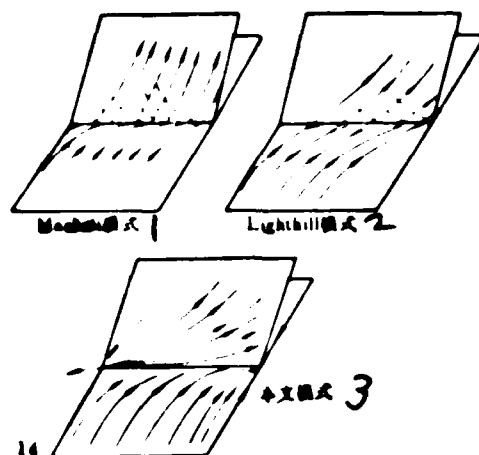


Fig. 14. Illustrations of the Alignment of Extreme Limit Flow Lines in Three Different Types of Models. 1. Maskell Model. 2. Lighthill Model. 3. The Model in This Article.

4. A discussion concerning upward flow line singularity points perpendicular to separation line cross sections. Due to the fact that separation planes are formed from flow lines which come out from points of singularity which are nodal points that appear on cross sections perpendicular to separation lines, when they intersect cross sections (sections above the surface of objects) perpendicular to separation lines, it forms a break line (the os line in Fig. 12(b)). Due to the fact that extreme limit flow lines, on lines of separation, do not turn up again, on cross sections perpendicular to separation lines, they form respectively straight lines from the two sides pointing toward intersection points, for example, Ao and Bo in Fig. 12(b), which give rise to the appearance of half saddle points.

III. Conditions Which Should Be Satisfied in the Vicinity of Separation Lines

We have already explained that separation lines are both surface shear lines and extreme limit flow lines. If we take the separation line as the y axis with the x axis perpendicular to the separation line (separation line coordinate system), the corresponding shear force components are τ_x, τ_y . On the separation lines, $\tau_y \neq 0, \tau_x = 0$. 338

Along the x direction, the shear force component τ_x changes sign in the vicinity of separation lines. Because of this, $\partial \tau_x / \partial x < 0$. It follows from this that

$$\tau_x = 0, \quad \partial \tau_x / \partial x < 0 \quad (11)$$

This is a necessary condition for three-dimensional separation. However, the condition described above does not consider the influence of changes in shear stresses along the direction of lines of separation.

Consider for a moment the situation of normal velocity w in the vicinity of separation lines. In order to do this, let us take a certain point P , on a separation line. Let us also take a point R , which is at a distance Δz from the separation line. For convenience sake let us choose point P , as the origin point. Then, the normal velocity at point R can be represented as

$$w_R = w_P + \left(\frac{\partial w}{\partial z} \right)_P z + \frac{1}{2} \left(\frac{\partial^2 w}{\partial z^2} \right)_P \Delta z^2 + \dots \quad (12)$$

From the continuity equation

$$\frac{\partial u}{\partial x} + \frac{\partial v}{\partial y} + \frac{\partial w}{\partial z} = 0 \quad \text{that is} \quad \frac{\partial w}{\partial z} = - \left(\frac{\partial u}{\partial x} + \frac{\partial v}{\partial y} \right) \quad (13)$$

On wall surfaces we have

$$w_P = 0, \quad \left(\frac{\partial u}{\partial x} \right)_P = \left(\frac{\partial v}{\partial y} \right)_P = 0$$

Because of this

$$\left(\frac{\partial w}{\partial z} \right)_P = - \left[\left(\frac{\partial u}{\partial x} \right)_P + \left(\frac{\partial v}{\partial y} \right)_P \right] = 0$$

Due to this

$$\left(\frac{\partial^2 w}{\partial z^2} \right)_P = - \left[\left(\frac{\partial^2 u}{\partial z \partial x} \right)_P + \left(\frac{\partial^2 v}{\partial y \partial z} \right)_P \right]$$

Therefore

$$w_R = - \frac{1}{2} \left[\left(\frac{\partial^2 u}{\partial z \partial x} \right)_P + \left(\frac{\partial^2 v}{\partial y \partial z} \right)_P \right] \Delta z^2 \quad (14)$$

It is required that, at the time of separation, $w_r > 0$. Because of this, it is required that

$$(\partial^2 u / \partial z \partial x)_r + (\partial^2 v / \partial y \partial z)_r < 0 \quad (15)$$

That is, for each point on the separation line, one should have

$$(\partial \tau_x / \partial x) + (\partial \tau_y / \partial y) < 0 \quad (16)$$

One can see from this that, in the vicinity of three-dimensional separation lines, the conditions which should be satisfied are

$$\tau_z = 0, \quad \frac{\partial \tau_x}{\partial x} < 0, \quad \frac{\partial \tau_x}{\partial x} + \frac{\partial \tau_y}{\partial y} < 0 \quad (17)$$

Reference [6], in solving for saddle points on cross sections, makes use of the condition $w_r > 0$. However, it does not take equation (16) and substitute into it the conditions which should be satisfied for three-dimensional separation. Below, we discuss the necessity of satisfying the condition $(\partial \tau_x / \partial x) + (\partial \tau_y / \partial y) < 0$.

As far as closed type separation is concerned, that is, the situation in which the point of origination is a saddle point and the end point is the separation nodal point, we still select a separation line coordinate system. Moreover, we assume that A, B , respectively are the initial and final points of singularity (Fig. 15). If there is a flow line through A, B , and the direction of that flow line is from A to B , then, on this flow line, changes in the rules for $\tau_x, \tau_y, \partial \tau / \partial y$ for various points should be as shown in Fig. 15. The line of separation is just this type of flow line.

As far as $\partial \tau_y / \partial y > 0$ is concerned, this section must guarantee $(\partial \tau_x / \partial x) + (\partial \tau_y / \partial y) < 0$. It is then required that $\partial \tau_x / \partial x < -\partial \tau_y / \partial y$.

That is, it is not simply required that $\partial \tau_x / \partial x < 0$.

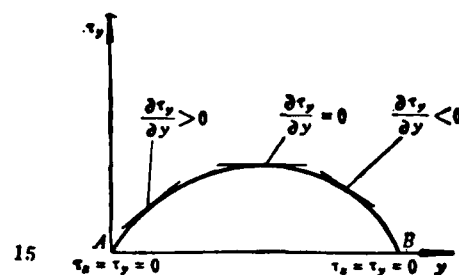


Fig. 15 Distribution of v_y Along Separation Line

Conclusion

As far as research on the criteria for three-dimensional separation goes, there is still a good deal of work that needs to be done. For example, the origination point for open form separation and its criteria. Even if one is dealing with closed form separation, the sufficient conditions for it have not yet been obtained. Following along with the development of calculations and experimental techniques, it is necessary to reach a deeper understanding among people of the phenomena produced by three-dimensional separation.

The various points of view in this article were discussed with such comrades as Zhang Hanxin and Wu Jiezhong, from which we obtained not a little instruction and profit. For this we express our thanks.

REFERENCES

- [1] Maskell, E. C., Flow Separation in Three Dimensions, Report Aero. 2565, (1955).
- [2] Tobak, M. and Peake, J. D. Topology of Two-Dimensional and Three-Dimensional Separated Flows, AIAA paper 79-1480, (1979).
- [3] Schlichting, H., Boundary Layer Theory, Tr. by J. Kestin, 6th ed., New York, McGraw-Hill, (1968).
- [4] Dallman, V., Three-Dimensional Vortex Separation Phenomena, AIAA paper 83-1735, (1983).
- [5] 吕志泳, 二元和三元定常分离的一些问题, 涡运动与分离学习班讲义, (1985).
- [6] 张涵信, 三维定常粘性流动的分流条件及分离线附近流动的性状, 空气动力学学报, 1985 年第一期, 第 1 页~12 页。

[5] Lu Zhiyong; "Several Questions Relating to Two Dimensional and Three Dimensional Separation," Lecture to the Study Team on Vortical Movements and Separation, (1985)

[6] Zhang Hanxin; "Flow Movement States in the Vicinity of Separation Flow Lines and Three-Dimensional Steady State Viscous Flow Movement Separation Conditions," Aerodynamics Journal 1985, No. 1, pp 1-12

STUDY OF THE SEPARATION CRITERION FOR STEADY 3-DIMENSIONAL VISCOUS FLOWS

Lü Zhiyong, Deng Xueying and Liu Mouji
(Beijing Institute of Aeronautics and Astronautics)

Abstract

In the case of steady, 2-dimensional separation, separation point is of a critical type. The limiting streamlines on the wall from both sides of the separation point run into the point and then depart away from the surface of the body with a certain angle. According to the definition of a critical point and the condition that the normal velocity closed to the separation point is non-zero, the separation criterion for steady, 2-dimensional flows can be deduced as follows: The friction stress at the separation point vanishes and There is a reversed flow after the separation. In the case of steady 3-dimensional separation, there is a separation line which starts at a saddle point and ends at a separated nodal point, as well as a separation sheet which consists of streamlines originating from a critical point. This critical point can be viewed as a saddle point topographically on the wall, or as an attached nodal point in the section containing the separation line and perpendicular to the wall. Based on the theory of singularities and topological rule, there may exist a half saddle point in the section cut normally to the wall and separation line. As a result, it can be argued that the argument about the limiting streamlines must rise before approaching separation line, due to Lighthill, is incorrect. This paper shows that the limiting streamlines along the wall always coincide with the corresponding friction lines. Limiting streamlines are attached to the wall until the separated nodal point or saddle point where they lift off the wall. Finally, the paper also presents the separation criterion for steady 3-dimensional flows which is different from that for 2-dimensional flows.

DETERMINATION OF OPTIMAL POSITION OF ACTUATORS
FOR FLEXIBLE FLIGHT VEHICLES

340

Yuan Jianping and Chen Shilu

(Northwestern Polytechnical University)

SUMMARY This article does research on the determination of optimal positions for control mechanisms in flexible aircraft. In control systems which have rate of speed feedback, the control function has been seen as an equivalent damping, and we have derived the criteria for optimal positions of the rudder face as determined by aerodynamic elasticity effects. We have also presented formulas for adjusting the relationships between the position of rudder surfaces and the position of gyroscopes. Practical examples are appended for empirical demonstration.

I. Introduction

Control mechanisms refer to control surfaces or oscillating engines. They can be abstractly conceived of as components producing concentrated forces or moments of force. The effects of control mechanisms are an important source of disturbance for the elastic vibration produced in aircraft. It can give rise to curvature or twisting vibration of aircraft structures. Therefore, it changes the size and distribution of aerodynamic forces in aircraft. It alters the efficiency of control surfaces and influences the control systems of aircraft. Differing installations of control mechanisms will produce differing results in the excitation of vibrations as far as elastic vibration movements are concerned. Because of this, the selection of optimum positions for control mechanisms has practical significance.

The purposes of making the positions of control mechanisms optimal are to be able, for general requirements, to reliably control aircraft movements and restrain elastic vibration. Such people as Gevarter [1] and Chen Shilu [2] did research on the influence of control mechanism positions and sensor positions on the stability of flexible aircraft. They made use of transmission functions and zero-polar methods respectively and discussed the conditions which should be satisfied by the locations of control

mechanisms and sensors. As a type of drive control method, such people as Arbel [3] and Schultz [4] presented an appropriate selection of location for control mechanisms in order to cause feedback systems to give rise to increases in flexible structure damping effects so as to facilitate the production by limited control of maximum restraining effects on elastic vibrations. However, all of them were dependent on numerical value calculations. They were not able to offer analytical relationships. This article, basing itself on the basic concept of the laws of aerodynamic energy, on the foundation of the work mentioned above, discusses a step further the question of the optimization of the location of elastic aircraft control mechanisms. In systems having velocity feedback, we derived two practical index functions and a simple relationship showing the adjustment positioning of rudder surfaces and gyroscopes. Moreover, it carries out empirical demonstrations using practical examples.

II. Optimum Position of Rudder Surfaces

This article considers the optimum position for rudder surfaces in control systems with velocity feedback. The equation describing the elastic vibration of aircraft, the measurement equation, and the control law are

$$\left. \begin{aligned} \ddot{q} + D_0 \dot{q} + K_0 q &= B_1 U + Q \\ Z_1 &= H_1 \dot{q} \\ U &= -G Z_1 \end{aligned} \right\} \quad (1)$$

In these, q is the generalized coordinate for elastic vibration. n is a dimensional vector quantity. D_0 is an $n \times n$ generalized, natural damping matrix. K_0 is an $n \times n$ generalized rigidity matrix. Q is an uncontrolled, generalized force. n_z is a dimension vector. Z_1 is the output vector for the r dimensional sensor. U is the m dimensional control vector. G is an $m \times r$ feedback matrix.

$$H_i = \begin{bmatrix} -\dot{\phi}'_1(\xi_i) & -\dot{\phi}'_2(\xi_i) & \dots & -\dot{\phi}'_n(\xi_i) \\ -\dot{\phi}'_1(\xi_i) & -\dot{\phi}'_2(\xi_i) & \dots & -\dot{\phi}'_n(\xi_i) \\ \dots & \dots & \dots & \dots \\ -\dot{\phi}'_1(\xi_i) & -\dot{\phi}'_2(\xi_i) & \dots & -\dot{\phi}'_n(\xi_i) \end{bmatrix} \quad (2)$$

$$B_i = \begin{bmatrix} F_{i1} & F_{i2} & \dots & F_{in} \\ F_{i1} & F_{i2} & \dots & F_{in} \\ \dots & \dots & \dots & \dots \\ F_{i1} & F_{i2} & \dots & F_{in} \end{bmatrix} \quad (3)$$

$\dot{\phi}'_i(\xi_i)$ expresses the value of a vibration mode derivative of order i at the location ξ_i of the number j sensor. F_{ij} expresses the shock force produced in order i vibration when the j -th control surface has a unit deflection. Let us assume that η_j is the coordinate along the vertical axis of the j -th control surface pressure center and that ρ_{j1} and ρ_{j2} are respectively the distances in the same direction from η_j to the forward and rear end points of this control surface. Then

$$\begin{aligned} F_{ij} &= -\frac{M}{m_i} \iint \frac{\partial^2 Z_{ij}}{\partial x \partial y} \phi_i(x, y) dx dy \\ &= -\frac{M}{m_i} \int_{\eta_j - \rho_{j2}}^{\eta_j + \rho_{j1}} dx \int_{y_1(x)}^{y_2(x)} \frac{\partial^2 Z_{ij}}{\partial x \partial y} \phi_i(x, y) dy \end{aligned}$$

M and m_i are respectively the mass of the aircraft and the generalized mass. Z_{ij} is the aerodynamic derivative for the j -th of the control surface. When handling the dispersion integrations described above, if the ratio between the effective rudder surface area and the characteristic surface area of the aircraft is very small, then it will approximate the form

$$F_{ij} = \lambda \phi_i(\eta_j) / m_i \quad (4)$$

λ is a constant relating to the coefficient of non-radiation characteristic area, and lift.

Because of this, in the closed loop system described in (1), the effect of feedback introduces into the system a quantity $(-B_1GH_1)q$.

For any arbitrary values of ξ , η , we have

$$B_1GH_1 = -\frac{1}{2}(B_1GH_1 + H_1^T G^T B_1^T) + \frac{1}{2}(B_1GH_1 - H_1^T G^T B_1^T)$$

In the equation above, the first section of the right hand side is symmetrical. It is the feedback coefficient which causes the system to have an energy exchange with the environment. It can be understood as the dissipation section. The second section is asymmetrical. It causes the system not to have an energy exchange with the environment. It can be understood as the inertial section (or gyroscopic section). Because of the fact that for any arbitrary value of q , the quadratic form $(B_1GH_1 - H_1^T G^T B_1^T)q$ is always zero, in terms of its physical meaning, the sum of the work done by force $(B_1GH_1 - H_1^T G^T B_1^T)q$ in any infinitely small real displacement dq , is zero. Let us say that

$$D_1 = B_1GH_1 + (B_1GH_1)^T \quad (5)$$

Then, we can recognize that $\frac{1}{2}D_1\dot{q}$ is the equivalent damping force controlling elastic vibration in the system. In order to have the greatest restraining effect on elastic vibration in the system, we suggest that the index of selection for the position of the rudder surface η be such as to make $J = \int_0^{t_1} (\dot{q}^T(t) D_1 \dot{q}(t)) dt$

(6)

is large is possible. In this case, when at the end of the movement of a certain load a disturbance q_1 is applied, completion of the transition process. In the case of such systems, after completion of the transition process, we have $\dot{q} = 0$. In this case, we need only compare, within the same area, i.e., $(t_1 - t_0)$ the speed of reduction of elastic vibration for different η . The precision of t_0 and t_1 does not have important significance.

The Rayleigh quotient of the definition matrix D_0

$$R(q) = \frac{\dot{q}^T D_0 q}{\dot{q}^T q}, \quad |\dot{q}| \neq 0$$

342

Making use of the nature of the extreme values of the Rayleigh quotient, it is possible to make the calculations below with the index (6) formula. Assume that the characteristic roots for the real symmetrical matrix D_0 are $\lambda_1 \leq \lambda_2 \leq \dots \leq \lambda_n$. Because of this

$$\begin{aligned} \min R(q) &= \lambda_1 \\ \max R(q) &= \lambda_n \end{aligned}$$

The index (6) formula satisfies

$$\lambda_1 \int_{t_0}^{t_1} (\dot{q}^T \dot{q}) dt \leq J \leq \lambda_n \int_{t_0}^{t_1} (\dot{q}^T \dot{q}) dt$$

Obviously, if λ_1 is non-negative, then, for any arbitrary values of q and $t_1 \geq t_0$, index J is also non-negative. At this time, the feedback system, speaking in terms of elastic movements, is stable.

In order to make description convenient, let us assume that the system has one velocity gyroscope and a pair of rudder surfaces. We will only consider third order vibration forms. Because of this G is a scalar quantity. We use d_{ij} to represent the elements of D_0 . From formula (2) to formula (4), we have

$$D_0 \equiv \begin{bmatrix} d_{11} & d_{12} & d_{13} \\ d_{12} & d_{22} & d_{23} \\ d_{13} & d_{23} & d_{33} \end{bmatrix}$$

$$\equiv -\lambda G \begin{bmatrix} 2 \frac{\phi_1(\eta)\phi'_1(\xi)}{m_1} & \frac{\phi_1(\eta)\phi'_2(\xi)}{m_1} + \frac{\phi_1(\eta)\phi'_1(\xi)}{m_2} & \\ \frac{\phi_1(\eta)\phi'_2(\xi)}{m_1} + \frac{\phi_2(\eta)\phi'_1(\xi)}{m_2} & 2 \frac{\phi_2(\eta)\phi'_2(\xi)}{m_2} & \\ \frac{\phi_1(\eta)\phi'_3(\xi)}{m_1} + \frac{\phi_3(\eta)\phi'_1(\xi)}{m_3} & \frac{\phi_2(\eta)\phi'_3(\xi)}{m_2} + \frac{\phi_3(\eta)\phi'_2(\xi)}{m_3} & \\ \frac{\phi_1(\eta)\phi'_3(\xi)}{m_1} + \frac{\phi_3(\eta)\phi'_1(\xi)}{m_3} & \frac{\phi_2(\eta)\phi'_3(\xi)}{m_2} + \frac{\phi_3(\eta)\phi'_2(\xi)}{m_3} & \\ \frac{\phi_2(\eta)\phi'_3(\xi)}{m_2} + \frac{\phi_3(\eta)\phi'_2(\xi)}{m_3} & 2 \frac{\phi_3(\eta)\phi'_3(\xi)}{m_3} & \end{bmatrix} \quad (5)$$

According to the nature of D_0 , it is possible to draw a few useful conclusions:

1. For any arbitrary values of ξ, η , we have $|D_0| = 0$. Because of this, D_0 at least has a zero characteristic root.

2. The second degree fundamental form of D_0 is $\begin{vmatrix} d_{11} & d_{12} \\ d_{12} & d_{22} \end{vmatrix} \equiv (d_{11}d_{22} - d_{12}^2) \leq 0$. If $(d_{11}d_{22} - d_{12}^2) \neq 0$, then, matrix D_0 is useful. It has one each positive, zero, and negative characteristic roots. When considered as a damping force, $D_0 \dot{q}$, in certain circumstances, creates a damping effect, and, in other circumstances, creates an accelerating effect. The overall effect is determined by the ratio relationships between the three roots.

3. If $d_{11}d_{22} - d_{12}^2 = 0$, then,

$$\frac{m_1 \phi_1'(\xi)}{m_2 \phi_2'(\xi)} = \frac{\phi_1(\eta)}{\phi_2(\eta)}$$

And, for $d_{11} > 0$

then, D , is semipositive and, for any value of q , one always finds $\partial D / \partial q = 0$. Moreover, when q is not zero, it is only at restricted single points that the equal sign appears. At this time, the form D, q is able to have a damping effect in the entire process.

4. If, at the same time the formula is satisfied, $d_{11} < 0$, then, D , is semi-negative, controlling the system so it always induces divergence.

To summarize what we have said, formula (7) and formula (8) describe the relationships adjusting the positions of the rudder surfaces and the gyroscopes. When ξ, η satisfy formula (6) and formula (8), it is possible to say that, in terms of aerodynamic elasticity, the entry and exit components of the system reach optimal design locations. From formula (7) and formula (8), it is possible, when rudder position is already known, to solve for optimum gyroscope position. On the other hand, it is also possible, for known gyroscope positions, to solve for optimum rudder positions. In the design process in general, one sets out initially from the control capability requirements for rigid aircraft, to specify rudder surface positions.

We will consider a general situation. Let us assume that the aerodynamic system is capable of being described by the use of the Lagrange equation:

$$\frac{d}{dt} \left(\frac{\partial W}{\partial \dot{x}_i} \right) - \frac{\partial W}{\partial x_i} = Q_i(t, \bar{x}, \dot{\bar{x}}), \quad i = 1, 2, \dots, n$$

In this equation, \bar{x}_i is a generalized coordinate for undisturbed movement, $\dot{\bar{x}}_i = \frac{d\bar{x}_i}{dt}$, $\bar{x} = (\bar{x}_1, \bar{x}_2, \dots, \bar{x}_n)^T$, W is the kinetic energy of the system $\bar{x}_i, \dot{\bar{x}}_i$, Q_i is the generalized force. When we consider the disturbances of $\bar{x}_i, \dot{\bar{x}}_i$, we respectively use $(\bar{x}_i + x_i)$ and $(\dot{\bar{x}}_i + \dot{x}_i)$ to replace \bar{x}_i and $\dot{\bar{x}}_i$ in formula (9). With just a little rearranging, formula (9) can become

$$\sum_{j=1}^n (a_{ij}\ddot{x}_j + b_{ij}\dot{x}_j + c_{ij}x_j) = y_i, \quad i = 1, 2, \dots, n \quad (10)$$

In this, $a_{ij} = a_{ji}$, y_i are the non-linearity terms for x_i and its derivative.

Let

$$\begin{aligned} b_{ij} &= \frac{1}{2}(\beta_{ij} + \beta_{ji}), & p_{ij} &= \frac{1}{2}(\beta_{ij} - \beta_{ji}), \\ c_{ij} &= \frac{1}{2}(\gamma_{ij} + \gamma_{ji}), & e_{ij} &= \frac{1}{2}(\gamma_{ij} - \gamma_{ji}). \end{aligned}$$

Take the n equations contained in formula (10) and write them in matrix form as

$$A\ddot{X} = -BX - CX - EX - PX + Y \quad (11)$$

In this equation:

$A = (a_{ij})$ is the generalized mass matrix, symmetrical, fixed positive

$B = (b_{ij})$ is the generalized damping matrix, symmetrical

$C = (c_{ij})$ is a generalized conservation of force coefficient matrix, symmetrical

$E=(e_{ij})$ is the radial correction force matrix, asymmetrical

$P=(p_{ij})$ is the gyroscopic force matrix, asymmetrical

Introducing the Rayleigh dissipation function

$$\tilde{F} = -\frac{1}{2} \dot{X}^T B \dot{X}$$

In this case, the drag force in formula (11) can be written as $\partial \tilde{F} / \partial \dot{X}$. Using an orthogonal transformation, we take \tilde{F} and change it into a square sum form

$$\tilde{F} = -\frac{1}{2} \sum_k b_k \dot{x}_k^2$$

If $b_k > 0$, then, force $b_k \dot{x}_k$ causes the movement to reduce speed. On the other hand, if $b_k < 0$, then $b_k \dot{x}_k$ causes the movement to increase speed. Therefore, the force derived from \tilde{F} may be of a dissipating form. It is also possible for it to be of an accelerating form. If $\sum_k b_k > 0$, then, one can say that, in the system as a whole, the dissipating forces are in a dominant position over the accelerating forces.

On the basis of the Lyapunov theorem, it is possible to know that, if acceleration forces are dominant over dissipating forces, then, the system described in formula (10) is unstable. If the determinant form $\gamma_{ij} < 0$, then, the aerodynamic system in formula (10) is also always unstable. These two points respectively provide basic principles for our selection of velocity feedback and displacement feedback in control systems.

344

Because of the fact that orthogonal transformations maintain matrices invariable, that is, $\sum_k b_k = \sum_j \tilde{b}_j$, it follows that there is no need to take B and change it into a diagonal matrix. We define a new function index

$$J = \text{tr.}(B) \quad (12)$$

In this, tr. expresses the matrix trace (trace). In order to cause the system to have maximum drag effects on disturbing movements, the selection of system parameters should cause J to become extremely large. When only considering gyroscope position and rudder surface position, it is possible to use D , as defined by formula (5) to replace B , in formula (12). Moreover, in the simple situation represented by formula (5)', it is possible to write the obvious form:

$$J = -\lambda G[\phi'_1(\xi) \phi'_2(\xi) \phi'_3(\xi)] \begin{bmatrix} \frac{1}{m_1} & & \\ & \frac{1}{m_2} & \\ & & \frac{1}{m_3} \end{bmatrix} \begin{bmatrix} \phi_1(\eta) \\ \phi_2(\eta) \\ \phi_3(\eta) \end{bmatrix} \quad (12)'$$

III. Actual Examples of Research

This section discusses elevator position on a certain type of aircraft. It is necessary to stress the fact that changes in rudder position have very great effects on the rigid control capabilities of aircraft. Because of this, the selection range for the parameter η is extremely limited. Moreover, after selecting it, it is necessary to correct the changes in rigid aerodynamic parameters in order to guarantee their being within permissible ranges.

We already know that the relevant data for this aircraft are: Gyroscope position $\xi = 5.45\pi$; rudder surface position $\eta = 6.54\pi$.

Vibration form $\phi_1(\eta) = 0.341$, $\phi_2(\eta) = -0.032$, $\phi_3(\eta) = -0.282$.

Vibration form derivatives $\phi'_1(\xi) = -0.36$, $\phi'_2(\xi) = 0.07$, $\phi'_3(\xi) = 0.25$.

Generalized mass $m_1 = 14.32$, $m_2 = 6.98$, $m_3 = 8.48$.

1. If we give η a somewhat different value, and the other data use current values for the aircraft, under conditions satisfying equation (1), we calculate the indices for formula (6). The results are shown in curve *A*. in Fig. 1. It is possible to see that, when η is in the range 6.4-6.85, all are possible. When $\eta=6.5$ J reaches an extremely large value. The results of calculations demonstrate that, when the rudder surfaces lie close to head section or tail section, the system diffuses. This explains the control system's continuous introduction of energy to the elastic movements.

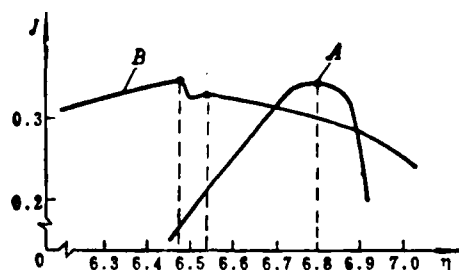


Fig. 1 Curves for Values of J for Changes in η . Calculated According to Different Indices

2. On the basis of formula (7), when we already know the generalized mass and gyroscope position, the optimum position for the rudder surface is at the location where the vibration form should satisfy

345

$$\phi_1(\eta)/\phi_2(\eta) = -10.55$$

We can find from the experimentally determined curves for (η) , that there are three values of η which satisfy the formula above: 1.08; 4.16; 6.48. $\eta = 1.08$ is not permitted by rigid body control capabilities. $\eta = 4.16$ does not satisfy formula (8). We eliminate these two roots. The results for $\eta = 6.48$ are in the ranges obtained in Fig. 1. Moreover, there is only a difference of 0.06 from current values. This method is simpler and more effective.

3. We make calculations from the index (12) formula. Given a somewhat different value for η , and using the values already given for $m_i, \phi_i'(\xi)$, the results are as seen in curve .B. in Fig. 1. At the place where $\eta = 6.48$, J reaches its maximum value. This is the same as the result from formula (7). Besides this, at the place where $\eta = 6.54$, one sees the appearance of a secondary maximum value. This agrees with the current values for this aircraft very well. In calculations other than these, there is no need to integrate the movement equations. To say it another way, the index (12) formula only depends on aircraft structural characteristics (mass distribution, vibration forms, and vibration form derivatives.)

Attention should be paid to the existence of a difference between the results obtained on the basis of the principle of formula (6) and those obtained from formula (12). The reason for this is that the calculations from the index (6) formula include a numerical value integration of equation set (1). In it, there is necessarily a calculation error. However, it is the first type of method, as compared to the other two types of methods, which requires the use of broad ranges of values.

The calculations above show that, starting from the restraining of elastic vibrations, the optimum rudder surface position should be at a distance 6.48 m from the head section. This position is moved forward 0.06 m from the design position in the original rigid body model. This will cause the control moment of force parameter and the drag moment of force parameter to go down respectively by 4% and 1.5%. Other dynamic parameters show no obvious changes.

IV. Conclusion

This article makes use of the concept of aerodynamic energy. It takes the effects of velocity feedback and sees them as equivalent to drag. We have derived the principles for optimum rudder surface locations with a view to restraining elastic vibrations. Index (6) formula and index (12) formula are appropriate for general use in velocity feedback control systems. In the simple situations which this article researches, formulas (7) and (8) can give simple and convenient results. Examples of practical research prove the

conclusions above. We obtained matching results from all three methods. Moreover, we demonstrated that the current rudder surface positions for aircraft being studied are secondary optimums.

REFERENCES

- [1] Gevarter, W. B., Basic Relations for Control of Flexible Vehicles, AIAA Paper 69-115 (1969).
- [2] 陈士椿等, 弹性飞行器纵向稳定性分析, 航空学报, 第六卷, 第四期(1985), 321~328页。
- [3] Arbel, A., Controllability Measures and Actuator Placement in Oscillatory Systems, INT. J. Control, Vol. 33, No. 3, (1981), pp. 565~574.
- [4] Schulz, G. and Heimbold, G., Dislocated Actuator/Sensor Positioning and Feedback Design for Flexible Structures, J. Guidance, Control & Dynamics, Vol. 6, No. 5, (1983), pp 361~367.

[2] Chen Shilu; "Analysis of Vertical Stability Characteristics in Elastic Aircraft"; Acta Aeronautica et Astronautica Sinica, Vol. 6, No. 4 (1985) pp. 321-328

DETERMINATION OF OPTIMAL POSITION OF ACTUATORS FOR FLEXIBLE FLIGHT VEHICLES

Yuan Jianping and Chen Shilu
(Northwestern Polytechnical University)

Abstract

Since the action of actuators on flexible flight vehicles is an important exciting source to elastic vibration, it is of practical significance to choose appropriate positions for actuators as well as for sensors. We shall in this paper study optimal positions of rate gyros and elevators that are modelled as lumped operating elements.

Through the feedback control, a term $(B_1 G H_1) \dot{q}$ is introduced to the system to count for the damping force, where B_1 is a control matrix, relying on the actuator locations, and H_1 is a measurement matrix depending on the gyro locations. An effective damping matrix D_e is defined in (5), and then Rayleigh's dissipation function can be obtained as $\tilde{F} = \frac{1}{2} \dot{q}^T D_e \dot{q}$. In order to make the system having most damping effect to vibration, the actuators and sensors are so positioned that the effective damping force $(\partial \tilde{F} / \partial \dot{q})$ could be maximized.

Because of its real symmetry, D_e can always be diagonalized. In accordance, suppose that $\tilde{F} = \frac{1}{2} \sum_k b_k \dot{q}_k^2$. If $b_k > 0$, the elastic motion will be decelerated by force $b_k \dot{q}_k$, if $b_k < 0$, the motion will be decelerated by force $b_k \dot{q}_k$, if $b_k < 0$, the motion will be accelerated. That is, the forces derived from \tilde{F} may be either dissipating or accelerating. When $\sum_k b_k > 0$, it is thought that the dissipating force is leading to the accelerating one.

Since the trace of a matrix will not be changed by a normal transformation, we have $\sum_k b_k = \text{tr. } D_e$. Then a new performance index is defined by (12). The problem under consideration is to determine the positions of actuators and sensors so that index (12) is maximized.

In general, the same results can be obtained from Lagrange's dynamic equations.

A simple condition has been studied. Through analysis, we have derived a set of simple and practical formulae (7) and (8) that give the very positions at which the effective damping force is always dissipating. By applying formulae (7) and (8) to a given missile, it is shown that the present position of the elevator is suboptimal and is 0.06m away from the optimal position.

NUMFRICAL SIMULATION OF A FLEXIBLE AIRCRAFT
TAKING-OFF AND LANDING ON UNEVEN RUNWAY

347

Rui Yuting

(Beijing Institute of Aeronautics and Astronautics)

SUMMARY This article does research on the use of Kane equations to set up a method of dynamic equations for flexible aircraft system including landing gear structures. It presents two types of models for the calculation of runway surfaces. After this, it discusses a numerical simulation method for the attitude, speed, acceleration, and dynamic loading of flexible aircraft during the process of taking off and landing. It does calculations of the effects on aircraft system dynamics of the inertial forces and inertial moments of force of all the major components of take-off and landing gear. To make a simple example, this article simulates the symmetrical take-off and landing of the KC-135 aircraft.

I. Introduction

When flexible aircraft are taking off and landing on uneven runways, their attitude, speed, acceleration, and dynamic loading are the main parameters for the design of landing gear, calculation of lift, and aircraft capabilities. Normally, these parameters are obtained through on-site measurements and high speed photography. The costs are high, and the time periods involved are long. Because of this, the use of computers to do a completely realistic numerical simulation in order to obtain these parameters is a problem worth re-searching.(1-3)

The numerical simulation of aircraft take-offs and landings primarily meets with the following three types of problems: (1) the mechanical model and dynamic equations for aircraft take-off and landing systems; (2) a calculation model for the surface of runways; (3) forms to express the effects of the ground surface on tire forces and aerodynamic forces.

Concerning the first problem, after the aircraft lowers its landing gear, the elastic fuselage, wings, and landing gear structures form a system with multiple degrees of freedom and multiple objects. If we calculate the effects on aircraft system dynamics of the inertial forces and inertial moments of force of all the major components of landing gears, then, in that case, when we use classical mechanical analysis methods to enumerate the dynamic equations of the system, we will meet with a difficult problem expressing complicated dynamics functions with forms involving multiple numbers and scalar quantities. At the present time, in references (1-3), doing research on the dynamic effects of symmetrical aircraft take-offs and landings, we take a wheelbarrow type landing gear and simplify it into a non-springy mass. Through springs and dampers, they are connected to the fuselage. As far as wheelbarrow type landing gear are concerned, this type of model did not consider the dynamic equation for the "curled up plate" form of wheelbarrow frame. During this process, dual directional shock absorbers must absorb a relatively large amount of energy. As far as rocker arm type landing gear are concerned, the movement characteristics and the dynamic characteristics of this type of model have relatively large differences from the actual components. Because of this, this article, first of all, does research on setting up a universal method using the mechanics equations for aircraft systems.

Concerning the second problem, the discussion in references (1-3) all deals with the calculation of the dynamic effects in the symmetrical take-offs and landings of aircraft. Therefore, they all assume an equivalent height at each point on the runway. Obviously, when simulating air craft take-offs and landings in any given situation, this type of assumption cannot reflect the actual situation. Because of this, there is a need to present a more reasonable calculation model.

Concerning the third problem, this article does not do any research. On the basis of the simulation of the first two problems, this article presents a numerical simulation method for aircraft take-offs and landings on uneven runways.

II. A Method for Setting Up Dynamic Equations in Aircraft Systems

Concerning systems composed of point masses and holonomic or first order non-holonomic multiple rigid bodies, T.R. Kane maintains that it is useless to solve dynamic functions. They do not have multiples, and, there is no need to consider the Kane formula for reactive restraints [4-5]

$$F_i + F_i^* = 0 \quad i = 1, 2, \dots, l - m \quad (1)$$

F_i is the generalized motive force for the system. F_i^* is the generalized inertial force for the system. l is the generalized coordinate number. m is the non-holonomic restraint. The method of solving for F_i and F_i^* under different circumstances can be seen in references [4-5].

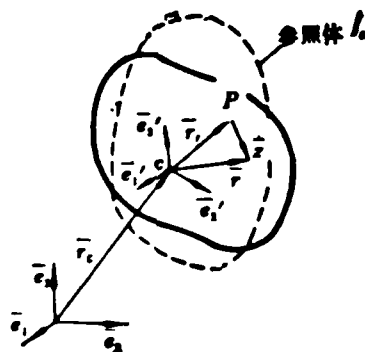


Fig. 1. Coordinate System and Elastic Main Body 1. Reference Body

Large aircraft, while taking off, landing, or taxiing on the ground, can be considered abstractly as main bodies and are elastic body multiple body systems. Elastic fuselage and wings are the principal bodies. The landing gear components, ailerons, and so on, are rigid body auxiliary components. Through generalized hinges, they are connected to the main body. One can see the main body as being the combination of an infinite number of point masses. The Kane

equation can be applied to this type of multibody system.

As is shown in Fig. 1, if we select the Tisserand reference system \bar{e}' to be the floating coordinate system for the main bodies, $\bar{e}'_1, \bar{e}'_2, \bar{e}'_3$ are three basic vectors for it. The position vector for a point P on the main body in the inertial coordinate system is $\bar{e}(\bar{e}_1, \bar{e}_2, \bar{e}_3)$

$$\bar{R} = \bar{r}_0 + \bar{r} + \bar{z} \quad (2)$$

In this equation, \bar{r}_0 is the position vector for the instantaneous center of mass of the main body. \bar{r} is the position vector for a point corresponding to a point \bar{z} on the reference body. P is the elastic displacement of point P .

The velocity and acceleration for point P are

$$\dot{\bar{R}} = \dot{\bar{r}}_0 + \bar{\omega} \times (\bar{r} + \bar{z}) + \dot{\bar{z}} \quad (3)$$

$$\ddot{\bar{R}} = \ddot{\bar{r}}_0 + \dot{\bar{\omega}} \times \bar{r} + \bar{\omega} \times (\bar{\omega} \times \bar{r}) + 2\bar{\omega} \times \dot{\bar{z}} + \ddot{\bar{z}} \quad (4)$$

$\bar{\omega}$ is the angular velocity of the reference body. $\bar{r} = \bar{r}_0 + \bar{r}_1, \dot{\bar{z}}$ and $\ddot{\bar{z}}$ represent respectively the first and second order derivatives of the relative coordinate system \bar{e}' versus time. If we assume that the generalized coordinate of the system is q_1, q_2, \dots, q_n , and the velocities set up for the system defined are u_1, u_2, \dots, u_n

$$\left. \begin{aligned} \bar{r}_0 &= \sum_{i=1}^3 \bar{e}_i u_i \\ \bar{\omega} &= \sum_{i=1}^6 \bar{e}'_i u_i \\ \dot{\bar{z}} &= \sum_{i=1}^n \bar{\phi}_i u_i \end{aligned} \right\} \quad (5)$$

This satisfies

$$(\ddot{u}_1, \ddot{u}_2, \dots, \ddot{u}_n)^T = A(\dot{q}_1, \dot{q}_2, \dots, \dot{q}_n)^T + A_1 \quad (6)$$

In this equation, $\bar{\phi}_i$ is the elastic modulus for the main body (looking at that in a convenient way, the subscripts i from 7 to n , are set up in such a way that $\bar{\phi}_i$ corresponds to the first order elastic modulus). A is an $l \times l$ order non-singular matrix. The elements of this and the l order line matrix A_1 are functions of the generalized coordinate versus time. From equations (3) and (5), we get the partial velocities for point P

349

$$\bar{v}_{i,j} = \begin{cases} \bar{e}_i & i = 1, 2, 3 \\ \bar{e}'_{i-3} \times \bar{r} & i = 4, 5, 6 \\ \bar{\phi}_i & i = 7, 8, \dots, n \\ 0 & i = n+1, n+2, \dots, l \end{cases} \quad (7)$$

From the equation $(F_i^*) = - \int_V \bar{v}_{i,j} \cdot \ddot{\bar{R}}_j$ it is possible to derive the contribution made by the elastic main body to the generalized inertial force as being

$$(F_i^*) = \begin{cases} -m_0 \ddot{u}_i & i = 1, 2, 3 \\ - \sum_{j=4}^6 (\bar{e}'_{j-3} \cdot \bar{J} \cdot \bar{e}'_{i-3}) \ddot{u}_j + f_i^* & i = 4, 5, 6 \\ -\bar{m}_i \ddot{u}_i + f_i^* & i = 7, 8, \dots, n \\ 0 & i = n+1, \dots, l \end{cases} \quad (8)$$

In this equation, m_0 is the mass of the main body. \bar{J} is the inertia tensor of the main body. \bar{m}_i is the generalized mass of order i . The non-linear quantity f_i^* includes quantities second order and higher for the elastic displacement \bar{u} and the angular velocity $\bar{\omega}$ of the main body. When we are talking about aircraft in the act of taking off and landing, it is possible to know the subquantities \bar{u} and $\bar{\omega}$. If we ignore the higher order quantities, then,

$$f_i^* = 0, \quad i = 4, 5, \dots, n.$$

From equation $(F_i) = \int_V \bar{V}_{i,j} \cdot d\bar{F} \quad i = 1, 2, \dots, l,$ it is possible to derive the internal force contribution of the elastic main body to the generalized motive force, which is

$$(F_i) = \begin{cases} -\tilde{m}_i \tilde{\omega}_i^2 q_i & i = 7, 8, \dots, n \\ 0 & \text{remainder} \end{cases} \quad (9)$$

In this equation, $\tilde{\omega}_i$ is the i th order generalized frequency for the elastic main body.

In this system, the contribution of all rigid body parts to the generalized inertial force can be expressed as

$$(F_i^*) = - \sum_{j=1}^l \pi_{ij} \dot{u}_j - \pi_i \quad i = 1, 2, \dots, l \quad (10)$$

In this equation, π_{ij} and π_i are generalized coordinates as a function of the determined velocities and time.

On the basis of the basic formula $(F_i) = \bar{V}_{i,j} \cdot \bar{F} \quad i = 1, 2, \dots, l,$ we solve for all external forces acting on the system and for the contributions of all active restraining forces in the system on the generalized motive force. We take that and equations (8), (9), and (10) together and substitute them into Kane equations. We obtain the dynamics equation for the elastic body, multi-body system which is the main body

$$M(\dot{u}_1, \dot{u}_2, \dots, \dot{u}_l)^T = H \quad (11)$$

In this equation, M is a $l \times l$ symmetrical square matrix. H is an l order line matrix. Equation (6) and equation (11) form a $2l$ order non-linear differential equation system.

III. A Calculation Equation for Runway Surfaces

Case 1: In the case of straight line take-offs of aircraft, landings and ground surface take-off runs, it is possible to recognize that the tires on the three landing gears of the aircraft will make three mutually parallel movements in vertical planes. Therefore, when one is simulating the straight line take-off and landing of aircraft, it would be a good idea to measure, on the surface of the runway, $3 \times m$ grid point locations of height h_{ij} , $i = 1, 2, 3$, $j = 1, 2, \dots, m$.

If we look at figure 2(a), $2a$ in the Fig is nearly equal to the distance between the two primary landing gear on the left and right of the aircraft. The length of b should be fixed with a view to the wave length of the ups and downs of the runway. In reference [1], the selection is $b = 61\text{cm}$. We set up three one dimensional list functions $x_j, h_{1j}, x_j, h_{2j}, x_j, h_{3j}$, $j = 1, 2, \dots, m$.

We use one dimensional, three point equidistant interpolation values to solve for the heights for points at distance x , that is,

$$h_i(x) \quad i = 1, 2, 3.$$

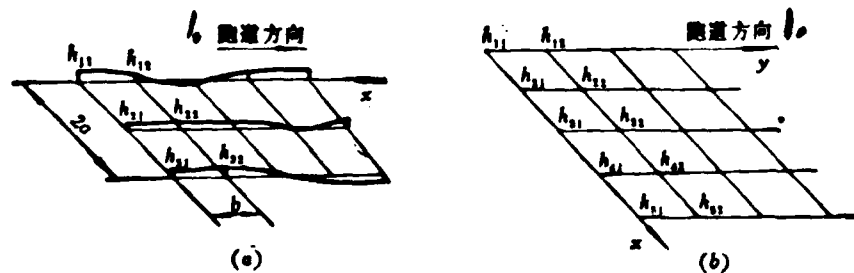


Fig. 2 A Calculation Model for Runways 1. Direction of Runway

Case 2: Because the initial position for aircraft take-offs and landings is random, and there are lateral aerodynamic forces and

deflection forces whose moments have effects on aircraft, in order to determine the height of any given location $h(x, y)$, we measure the height of a $15 \times m$ grid point h_{ij} , $i = 1, 2, \dots, 5$, $j = 1, 2, \dots, m$. As is shown in Fig. 2(b), we set up a two-dimensional equidistant list function and use a two-dimensional equidistant parabola-parabola interpolation to calculate $h(x, y)$.

IV. Ground Surface Forces and Aerodynamic Forces

Forces having effects on the tires can be analyzed into supporting forces along the vertical direction F_v , friction forces F_H and lateral forces F_s , which act on tires when aircraft are sliding through turns. F_v is determined through static pressure characteristic curves for the tires. F_H is determined from the integral motion equations for the rotation of the wheels of the aircraft or from storage friction forces. Below, we discuss the solution for the lateral forces F_s .

As is shown in Fig. 3, if we assume that the direction of the aircraft's forward landing gear wheels cannot be controlled, the lateral force which affects the main wheel on the left and the lateral force which affects the main wheel on the right are equivalent. The instantaneous rate of curvature radius for the track of the movement at a point C' between the left main wheel and the right main wheel is

$$\rho = \frac{a(V_{v1} + V_{v2})}{V_{v1} - V_{v2}} \quad (12)$$

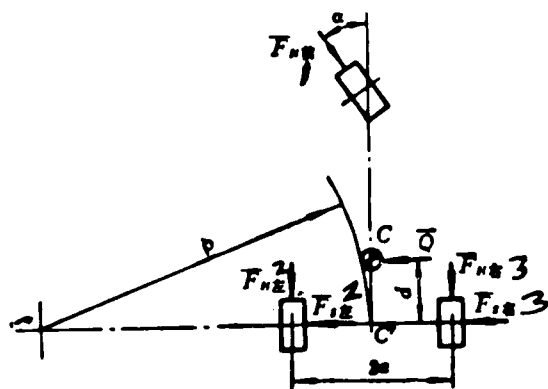


Fig. 3 Force Analysis for Aircraft Slide in Turns 1) Front 2) Left 3) Right

In this equation V_{left} (left) and V_{right} (right) represent respectively the movement velocities of the left and right main wheels. Speaking in general terms, the distance from the center of mass C to the point C' must be much smaller than ρ . For example, in the BOEING 707 aircraft $d = 1.32 \text{ m}$. In the BOEING 733-94 & 733-94 aircraft, $d = 1.27$. Therefore, we can know that the rate of curvature radius for the center of mass C is equal to the rate of curvature radius for point C' . In a natural coordinate system, the normal dynamics equation for the aircraft is

$$m \frac{V_c^2}{\rho} = 2F_L + Q - F_H \sin \alpha$$

In this equation, m is the mass of the aircraft. V_c is the velocity of the center of mass of the aircraft. Q is the horizontal component of the main aerodynamic force vector having an effect on the aircraft. From this equation, we can solve for

$$F_L = \frac{1}{2} \left(m \frac{V_c^2}{\rho} - Q + F_H \sin \alpha \right) \quad (13)$$

as an approximation calculation. In the interval of integration $[t_0, t_{n1}]$ we select $V_{cl} = V_{cln}$ and substitute into equation (13) to get $F_{Ll} = F_{Lln}$.

Aircraft, during the processes of take-off and landing, exhibit very large changes in velocity and are affected by ground surface forces which change from time to time. Because of this, aerodynamic lift forces should be calculated on the basis of abnormal aerodynamic forces when aircraft are making any movements. However, the problems involved in carrying out calculations for non-steady state aerodynamic forces when aircraft are making arbitrary movements are extremely complicated. This article, on the basis of references (3,7), introduces calculations of aerodynamic forces from steady state flow and laminar strip theory.

V. Simulation Methods

Let us consider the aircraft system composed of the elastic fuselage, wings, forward landing gear and two main landing gear. Assume that the wheelbarrow type landing gear is composed of the main column B_1 , the plunger B_2 , and the wheelbarrow or trolley frame B_3 (three rigid bodies). See Fig. 4(a). Assume that the rocker arm type landing gear with vibration reduction devices on the outside of the main column is composed of the main column B_1 , the rocker arm B_2 , the exterior vibration reduction device tube B_3 and the plunger B_4 . See Fig. 4(b). Let us further assume that the rocker arm type landing gear with vibration reduction devices inside the main column is composed of the main column B_1 , the rocker arm B_2 and the plunger B_3 . See Fig. 4(c). Aircraft on which the forward landing gear are rocker arm type and the main landing gear are wheelbarrow or trolley type or other types of aircraft are composed of different combinations of the three basic types of landing gear described above.

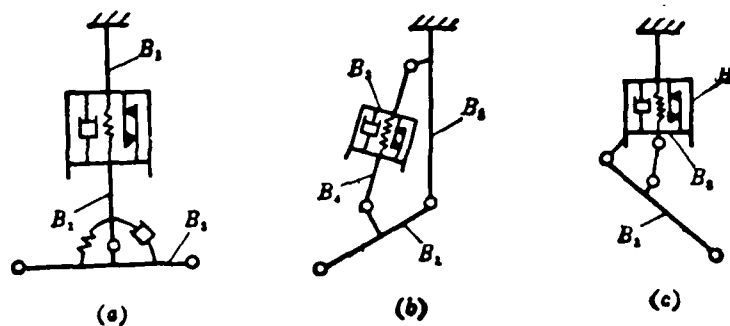


Fig. 4 Models of Landing Gear

The inertial coordinate system $\bar{e}(\bar{e}_1, \bar{e}_2, \bar{e}_3)$ is fixed on the surface of the ground. Its three basic axes run respectively along the horizontal direction of the runway, the horizontal

direction perpendicular to the runway, and the vertical direction. We select the Tisserand axis system $\bar{e}'(\bar{e}'_1, \bar{e}'_2, \bar{e}'_3)$ to be the reference axis system for measuring elastic deformations in aircraft. Its three basic axes correspond respectively to the two perpendicular horizontal axes and the vertical axis of the aircraft reference body. Let us assume that x, y, z is the origin point of \bar{e}' coordinate system. In coordinate \bar{e} , ψ, θ, φ are the three Klaylov angles. q_1, q_2, \dots, q_n are the generalized coordinates for the symmetrical and asymmetrical modalities of aircraft. s_1 is the travel path of the vibration reduction device on the forward landing gear. If one is dealing with a wheelbarrow or trolley type landing gear, then, the angle of rotation of E_1 relative to B_1 is β_1 . Corresponding to what was said above, the left main gear quantities are s_2 and β_2 . The right main gear quantities are s_3 and β_3 . With selected velocities,

$$\begin{pmatrix} \dot{u}_1 \\ \dot{u}_2 \\ \vdots \\ \dot{u}_i \\ \vdots \\ \dot{u}_n \end{pmatrix} = \begin{pmatrix} 1 & & & & \\ & 1 & & & \\ & & 1 & & \\ & & -S_\theta & 0 & 1 \\ & & C_\theta S_\varphi & C_\varphi & 0 \\ & & C_\theta C_\varphi & -S_\varphi & 0 \\ & & & & 1 \\ & & & & \ddots \\ & & & & & 1 \end{pmatrix} \begin{pmatrix} \dot{x} \\ \dot{y} \\ \dot{z} \\ \dot{\psi} \\ \dot{\theta} \\ \dot{\varphi} \\ \dot{q}_1 \\ \vdots \\ \dot{\beta}_1 \end{pmatrix} \quad (14)$$

In this equation, $S_\theta = \sin \theta$, $C_\theta = \cos \theta$, $S_\varphi = \sin \varphi$, $C_\varphi = \cos \varphi$.

Obviously, equations (5) and (6) are satisfied. When $\theta \neq \frac{\pi}{2}$ in the equation above, the square matrix A on the right side can be reversed.

On the basis of the previous discussion, we solve for the contributions of all the rigid body components of the front landing gear and the two main landing gear to the generalized inertial force. We solve for the contributions to the generalized motive force by aerodynamic forces, the ground surface forces affecting the tires, the gas pressure forces inside the vibration reduction devices, hydraulic drag forces and storage friction forces as well as trolley gear drag corresponding to the drag forces of main column rotation. If we assume that the elastic deformation of the aircraft and the angular velocity of the aircraft are small quantities, we ignore their small second order components. We consider the structural drag of the fuselage and the wings, and, in equation (11), the right side drag quantities are $(0, 0, 0, 0, 0, 0, \lambda_1 u_1, \lambda_2 u_2, \dots, \lambda_n u_n, 0, \dots, 0)^T$. Finally, we get the aircraft system dynamics equation

$$M(\dot{u}_1, \dot{u}_2, \dots, \dot{u}_n)^T = H \quad (15)$$

From equation (14), we get

$$(\dot{x}, \dot{y}, \dot{z}, \dot{\psi}, \dots, \dot{\beta}_3)^T = A^{-1}(u_1, u_2, \dots, u_n)^T \quad (16)$$

The equation set of (15) and (16) is simultaneously solved by integration using a computer.

Inside vibration reduction devices, there are storage friction forces F_{si} $i=1, 2, 3$. The subscripts 1, 2, 3 respectively represent the front landing gear, the left main landing gear, and the right main landing gear. Within the area of integration (t_1, t_{n1}) .

If

$$F_{si} < (F_{si})_{max} \quad i = 1, 2, 3$$

then, the vibration reduction devices are locked in. At this time, we add the restraining conditions

$$\begin{aligned} s_i &= s_i|_0, \quad i = 1, 2, 3 \\ \dot{s}_i &= u_{n+1,i-1} = \dot{u}_{n+2,i-1} = 0 \end{aligned} \quad (17)$$

We eliminate the $n+2i-1$ th equation from the equation set of (15) and (16).

VI. Sample Calculation

This article makes use of ATLSP (Airplane Take-off and Landing Simulation Program) simulation programming to make calculations of the process of symmetrical landings by KC-135 aircraft. Initially, aircraft data was taken from reference [2]. Runway data was taken from reference [1]. All missing parameters such as landing gear component mass and moment of inertia are supplied as assumed values. The increment of integration is taken as $\Delta t = 0.001 \text{ s}$. The reliability of the ATLSP programming is supported by large amounts of empirical measurements and experimentation carried out with domestically produced aircraft. We carried out a comparison of these with the calculation results from the simulation in order to verify it.

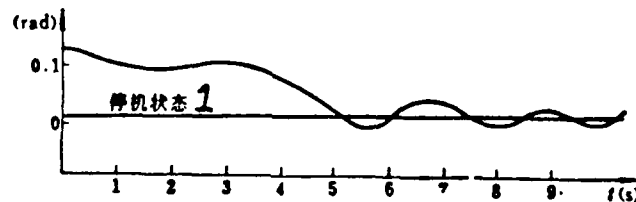


Fig. 5 Aircraft Angle of Pitch 1. Stationary Aircraft Configuration

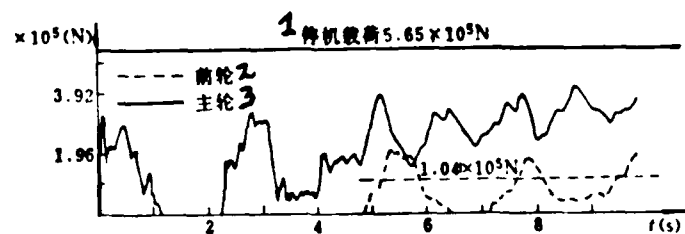


Fig. 6 Vertical Forces Influencing the Front Wheels and Main wheels
1. Stationary Aircraft Load 2. Front Wheel 3. Main Wheels

The aircraft assumes a landing speed of 71.6 m/s. It lands at a descent speed of 1.8 m/s. 3 seconds after main wheel touchdown, flight personnel pull the stick 5 degrees. Fig. 5 is the aircraft pitch angle-time curve. From this Fig we can see that, 5 seconds after the aircraft lands, it reaches the pitch angle for a stationary aircraft. After this, it oscillates in a decaying sine wave form. Fig. 6 is the load-time curve for the load affecting the front wheel and main wheels. From Fig. 6 we can see that, after the aircraft first touches the ground, it bounces and leaves the ground. Then, it executes a second landing. The vertical forces affecting the main wheels at the moment of impact are certainly not maximum. Fig. 7 is

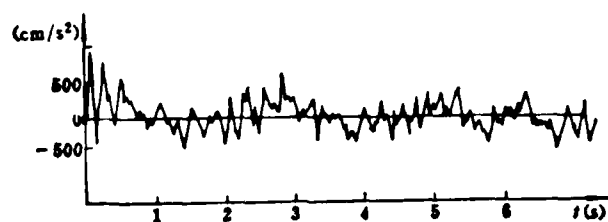


Fig. 7 Vertical Acceleration at Point C'

the vertical acceleration-time curve for the position p (i.e. C) of the center of mass of the aircraft. Fixed at a point on the curve P , that is the instantaneous center of mass of the aircraft.

Acknowledgments

This article was completed with the valuable advice given by Professor Hwang K-hsi and Assistant Professor Kie Shun-feng. Moreover, we have obtained the earnest help of Chuang-chi Kuo-pen. For this, we express our sincere gratitude.

References

- [1] Tung, C. C., Penzien, J. and Horonjeff, R., The Effect of Runway Unevenness on the Dynamic Response of Supersonic Transports, NASA CR-119 (1964)
- [2] Anthony G. Gerardi and Adolph K. Lohwasser, Computer Program for the Prediction of Aircraft Response to Runway Roughness, AD-786 490 (April, 1974)
- [4] Kane, T. R. and Likins, P. W., Spacecraft Dynamics, McGraw-Hill Book Co. (1983)
- [5] Kane, T. R., Dynamics of Nonholonomic Systems, Transactions of the ASME, J. of Applied Mechanics (1961), pp574-578
- [3] Ni Xueren; "Time-Dependent Position Vector for the Affected on Aircraft of Symmetrical Landing Shock and Curved Run"; Contribution to China Aeronautical Science and Technology, vol. 2000, 1982.
- [6] Wittenberg, J., Author; trans. Xia Guo-feng; "Multi-Body System Dynamics"; Publishing House, Beijing Aeronautical Institute, (1986)
- [7] Fuxin, H.W., Author; trans. Chen Kiyang; "Principles of Aerodynamic Elastic Mechanics"; Shanghai Science and Technology Publishing House; (1982)

NUMERICAL SIMULATION OF A FLEXIBLE AIRCRAFT TAKING-OFF AND LANDING ON UNEVEN RUNWAY

Rui Yuting

(Beijing Institute of Aeronautics and Astronautics)

Abstract

The method of using Kane's equation to develop the dynamic equations of a flexible aircraft system including landing gear mechanisms is investigated in this paper. Two kinds of mathematical models of runway surface are given. Then, the numerical simulation method is discussed for simulating the attitude, velocities, accelerations and dynamic loads of a flexible aircraft during take-off and landing, taking into account of the effect of inertial forces and moments of large landing gear parts on the motion of the system. As a simple example, the symmetric take-off and landing of KC-135 aircraft on the runway No. 12 is simulated. The numerical results are only for reference.

END

8-87

DTIC